Cell Metabolism

Amygdala NPY circuits promote the development of obesity under chronic stress conditions

--Manuscript Draft--

Manuscript Number:	CELL-METABOLISM-D-18-00379R3
Full Title:	Amygdala NPY circuits promote the development of obesity under chronic stress conditions
Article Type:	Research Article
Keywords:	NPY, central amygdala, stress, feeding, obesity
Corresponding Author:	Herbert Herzog, PhD Garvan Institute of Medical Research Sydney, NSW AUSTRALIA
First Author:	CHI KIN IP, Ph.D
Order of Authors:	CHI KIN IP, Ph.D
	Lei Zhang
	Aitak Farzi
	Yue Qi
	Ireni Clarke
	Felicia Reed
	Yan-Chuan Shi
	Ronaldo Enriquez
	Chris Dayas
	Bret Graham
	Denovan Begg
	Nicola Lee
	Jens C Brüning
	Gopana Gopalasingam
	Julia Koller
	Diana Hernandez-Sanchez
	Ramon Tasan
	Günther Sperk
	Herbert Herzog
Abstract:	Neuropeptide Y (NPY) exerts powerful feeding related functions in the hypothalamus. However, extra-hypothalamic nuclei also produce NPY but its influence on energy homeostasis is unclear. Here we uncover a previously unknown feeding stimulatory pathway that is activated under conditions of stress in combination with calorie dense food with NPY neurons in the central amygdala being responsible for an exacerbated response to a combined stress and high fat diet intervention. Central amygdala NPY neuron specific Npy overexpression mimics the obese phenotype seen in a stress/high fat diet model, which is prevented by the selective ablation of Npy. Using food intake and energy expenditure as readout we demonstrate that selective activation of central amygdala NPY neurons results in increased food intake and decreased energy expenditure, which requires the presence of NPY. Mechanistically it is the diminished insulin signalling capacity on central amygdala NPY neurons under stress/high fat diet conditions that leads to the exaggerated development of obesity.

Suggested Reviewers:	Michael Cowley, BSc (Hons) (Melbourne), PhD (Monash) Department head, Monash University michael.cowley@monash.edu Professor Michael Cowley is an Australian physiologist. He is best known for his mapping of the neural circuits involved in metabolism, obesity and diabetes treatment.
	Richard Palmiter, Ph.D Laboratory head, University of Washington palmiter@uw.edu Professor Richard Palmiter is an expert in using mouse genetic models and viral gene transfer to dissect neural circuits involved in different innate behaviours including feeding.
	Marcelo de Oliveira Dietrich, MD, PhD Assisstant professor, laboratory head, Yale school of medicine marcelo.dietrich@yale.edu Professor Dietrich is an expect in the neuroendocrine field, with his MD background on neurobiology.
	Patricia de Oliveira Prada, Ph.D Laboratory head, State University of Campinas pprada@fcm.unicamp.br Dr Prada has published multiple papers on neuronal insulin signalling, we thought she would have the expertise to review our paper.
Opposed Reviewers:	

Dear Dr Emambokus,

Thank you very much for assisting us to comply with the editorial requirements.

As requested we have now addressed the remaining editorial requirements and submit our final revised version following the given instructions.

Specifically we have amended:

a) We re-edited the summary down to 147 words.

b) In addition we have linked all the supplemental figures with at least one main item.

c) We generated a single PDF file to include all the Supplemental figures as well as their corresponding titles (including "Related to" information) and legends.

d) We have confirmed the Supplemental table has a descriptive title, as well as now including the "Related to" information, in the main manuscript file, after the STAR Methods section.

e) We have edited our fourth highlights and the new version contains only 79 characters including space.

f) Graphical abstract has been edited according to the requirement.

g) A declaration of interest form has been completed.

We trust that this changes now satisfactory address all the remaining editorial issues and the article is suitable for final acceptance.

Sincerely

Herbert Herzog

Response to Reviewers

No further response to reviewers required.

Graphical Abstract PDF format

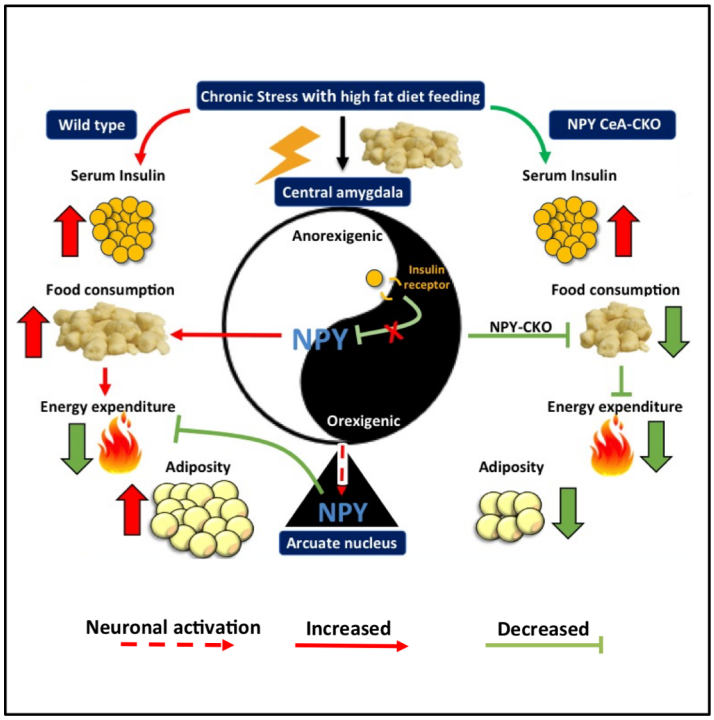

Graphical Abstract PNG format

Click here to access/download;Graphical Abstract;Edited graphical abstract 300 DPI.png

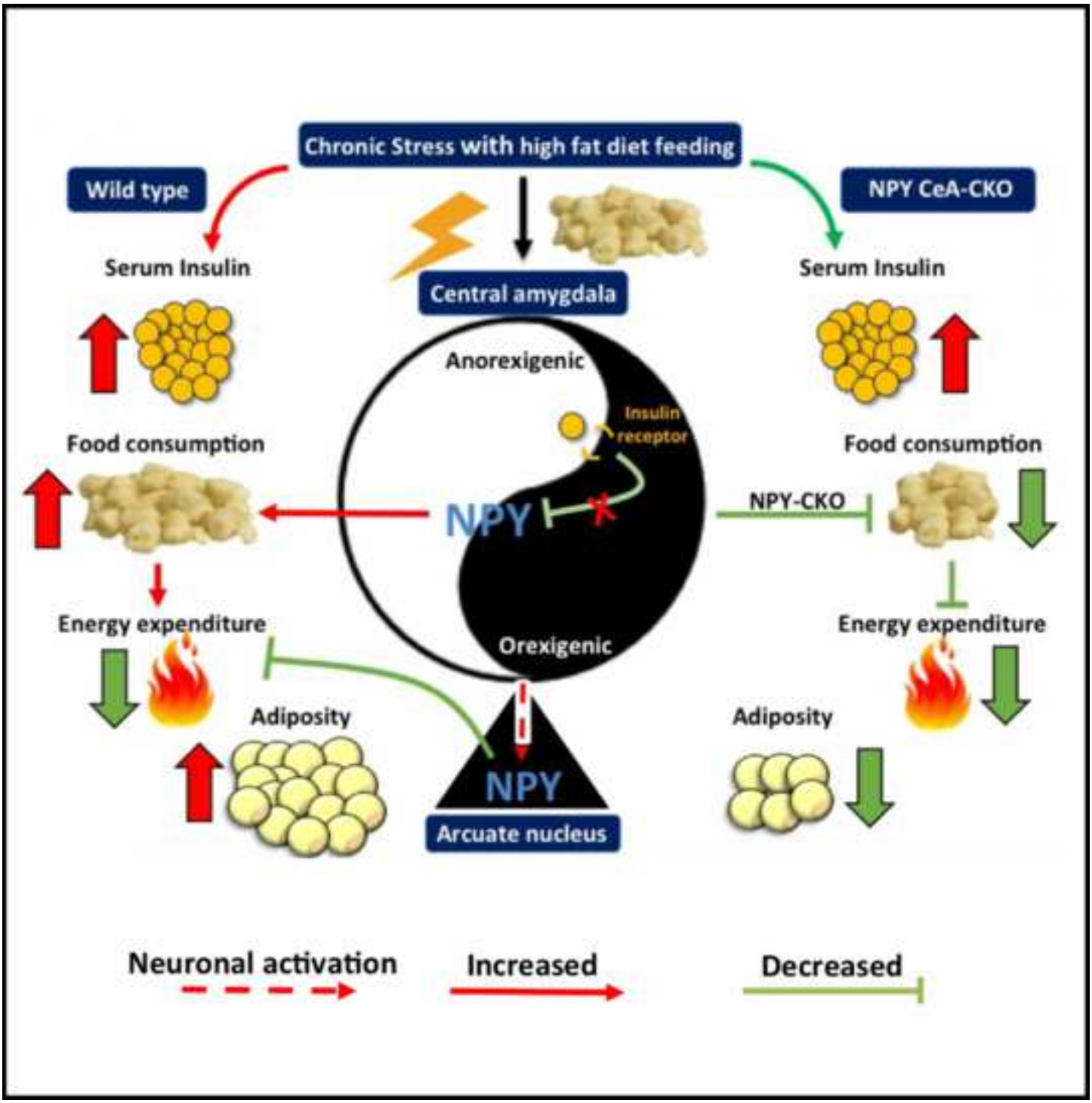

Amygdala NPY circuits promote the development of accelerated obesity under chronic stress conditions

Chi Kin Ip[1,2], Lei Zhang[1,2], Aitak Farzi[1], Yue Qi[1], Ireni Clarke[1], Felicia Reed[1], Yan-Chuan Shi[1,2], Ronaldo Enriquez[1], Chris Dayas[3], Bret Graham[3], Denovan Begg[4], Jens C Brüning[5], Nicola J Lee[1,2], Diana Hernandez-Sanchez[1], Gopana Gopalasingam[1], Julia Koller[1], Ramon Tasan[6], Günther Sperk[6] and Herbert Herzog[1,2,*]

[1]Neuroscience Division, Garvan Institute of Medical Research, 384 Victoria Street, Darlinghurst, Sydney, NSW, 2010, Australia; [2]Faculty of Medicine, University of New South Wales, Sydney, NSW 2052, Australia; [3]School of Biomedical Sciences & Pharmacy, University of Newcastle, NSW Australia; [4]School of Psychology, University of New South Wales, Sydney, NSW, 2052, Australia; [5]Max Planck Institute for Metabolism Research, Cologne, Germany; [6]Department of Pharmacology, Medical University Innsbruck, 6020 Innsbruck, Austria.

Running title: Central Amygdala NPY promotes stress-induced obesity

Key words: NPY, central amygdala, stress, feeding, obesity

[*]Lead contact and corresponding author: h.herzog@garvan.org.au

SUMMARY

Neuropeptide Y (NPY) exerts powerful orexigenic effect in the hypothalamus. However, extra-hypothalamic nuclei also produce NPY but its influence on energy homeostasis is unclear. Here we uncover a previously unknown feeding stimulatory pathway that is activated under conditions of stress in combination with calorie-dense food with NPY neurons in the central amygdala being responsible for an exacerbated response to a combined stress and high fat diet intervention. Central amygdala NPY neuron specific *Npy* overexpression mimics the obese phenotype seen in a stress/high fat diet model, which is prevented by the selective ablation of *Npy*. Using food intake and energy expenditure as readouts we demonstrate that selective activation of central amygdala NPY neurons results in increased food intake and decreased energy expenditure. Mechanistically it is the diminished insulin signalling capacity on central amygdala NPY neurons under stress/high fat diet conditions that leads to the exaggerated development of obesity.

INTRODUCTION

The body constantly adapts to both psychological and physiological stressors to maintain homeostasis. While in acute stress this is adaptive, chronic stress has adverse consequences on many organ systems as well as on a variety of physiological processes including eating behaviour, adiposity and fat distribution. Animal studies have shown that stress can lead to an increase, but mostly to a decrease in food intake (Mcewen et al., 2004; Levine et al., 1981). In rats for example, the dose response relationship between stress and reduced food intake suggests that decreased food intake and weight loss can serve as reliable markers of stress severity (Morley et al., 1983). Importantly, however, when rats have access to palatable food, high in fat or sugar, stress significantly increases the intake of the palatable food (Armario et al., 2006; Dallman et al., 2003). In humans, stress also affects eating in a bidirectional way; while some individuals decrease their food intake and lose weight during or after stress, the majority of people actually increase their food intake during stress (Dallman et al., 2005; Epel et al., 2004). Furthermore, during times of stress, most people report an increase in the intake of highly palatable foods, independent of overall hyperphagia or hypophagia (Stone et al., 1994).

The hypothalamic-pituitary-adrenal (HPA) axis has been implicated in this process and is tightly intertwined with endocrine parameters that regulate appetitive behaviours. In addition to regulation by the circadian rhythm, studies have suggested that energy balance is also regulated by feedback loops involving glucocorticoids, insulin, leptin and neuropeptide Y (NPY) under acute HPA activation (Cavagnini et al., 2000). The interactions between these hormones facilitate the storage, distribution and release of energy according to needs and contribute to the initiation and termination of a meal. Under normal, unstressed circumstances insulin and glucocorticoids have antagonistic effects on metabolism in the periphery (Dallman et al., 1993), creating a finely balanced system in order to provide sufficient fuel for the organism proportionate to demands. Importantly, however, glucocorticoid response elements are also located within the promoter of the *Npy* gene itself (Cavagnini et al., 2000), suggesting a critical direct control of *Npy* expression under stress conditions. Furthermore, there is also evidence that in addition to glucocorticoids, insulin can directly control *Npy* expression particularly in the amygdala opening up an additional major pathway for NPY to influence energy homeostasis under stress conditions (Boghossian et al., 2009; Castro et al., 2013).

It is well established that NPY is an anxiolytic peptide, which is widely expressed in different amygdala subnuclei where its expression leads to decreased anxiety with the central and basolateral amygdala

being the critical sites for that action (Tasan et al., 2010; Wood et al., 2016). NPY has also been described as a regulator of 'emotional eating' due to its role in the response to stress in psychiatric disorders (Heilig et al., 2004; Kim et al., 2003; Yehuda et al., 2006). For example, low serum NPY concentrations have been found in subjects with post-traumatic stress disorder and depression (Heilig et al., 2004; Rasmusson et al., 2000), psychiatric conditions classically associated with a loss of appetite. Conversely, increased NPY is associated with stress resilience in subjects that have been exposed to traumatic experiences (Yehuda et al., 2006). Therefore, dynamic changes in *Npy* expression levels in the amygdala in response to stress may be an important biochemical signal underlying stress-dependent eating. Despite the role of amygdala-derived NPY in regulating fear and anxiety having been well studied, the part it plays in regards to the regulation of feeding and energy homeostasis is largely unknown. In order to understand the potential interaction between stress-related NPY expression in the central amygdala (CeA) and its influence on feeding we utilized a set of novel mouse models that allow for NPY neuron specific deletion or overexpression of *Npy* in an inducible adult-onset fashion, as well as the selective activation of insulin responsive amygdala NPY neurons to identify the network linking NPY neurons in the amygdala to critical areas in the hypothalamus that control energy homeostasis.

RESULTS

Phenotypic characterization of stress-induced obesity

To investigate the impact of chronic stress on the regulation of body composition and body weight under different diet conditions, 4 groups of mice A) chow-fed, no stress (Chow), B) chow-fed and stress (ChowS), C) high-fat-diet fed, no stress (HFD) and D) high-fat-diet fed and stress (HFDS), were tested in a comprehensive phenotyping paradigm. As an effective stressor we used our established methodology (Kuo et al., 2007; Zhang et al., 2014) which involves placing individual mice alone in a home cage in which the bedding has been replaced by 1 cm deep, 10 ^{o}C water where they can freely move about for 1 hour, 3 times per week, at T_A 21 ^{o}C (Fig 1A). This protocol induced a consistent stress response as shown by significantly increased serum corticosterone levels (Fig 1B). Consistent with the known effect of high fat diet on energy expenditure (EE), body temperature as measured by infrared monitoring of skin temperature over the brown adipose tissue (BAT) and lumbar spine region (Fig 1C) did increase in the HFD groups (Fig 1D, 1E). Importantly, however, the stress protocol itself did not influence body temperature with unaltered values observed in the stressed compared to unstressed animals on the same diet (Fig 1D, 1E).

In order to capture the early responses to these treatments and avoid the potential complications from compensatory effects that may occur during prolonged stress, the initial experiments were performed over a 2-week period. Animals were maintained on a HFD where 43 % of the calories came from fat. Importantly, after only 5 days of treatment, HFD compared to Chow mice began to show significant increases in body weight, both in absolute values (Fig 1F) as well as when expressed as body weight gain (Fig 1G). Mice on chow exposed to the stressor (ChowS) showed no difference in body weight compared to unstressed mice (Chow) throughout the 2-week period (Fig 1F, 1G). Importantly, when combining the highly palatable diet with the stressor, the HFDS group showed a significantly accelerated body weight gain and increased body weight compared to all other groups (Fig 1F, 1G). This significantly increased body weight gain in the HFDS group was almost entirely due to an increase in fat mass (Fig 1H). Although lean mass was not affected (Fig 1I), whole-body-mineral density (BMD) and bone-mineral content (BMC) were significantly reduced in the ChowS group (Fig 1J, 1K), consistent with the known negative impact of chronic stress on bone mass (Baldock et al., 2014; Zhang et al., 2014). Analysis of the weight of individual fat depots revealed that combined HFD and stress treatment promoted white adipose tissue (WAT) gain uniformly in all major depots, including inguinal (i), epididymal (e) mesenteric (m) and

perirenal fat (r), both in absolute values (Fig 1L) as well as when normalised to body weight (Fig S1A) without affecting other tissue weights (Fig S1B, S1C). While brown adipose tissue (BAT) weight was also increased by HFD feeding, it was not further changed in HFDS mice (Fig 1L). To exclude any impact of the 10 ^{o}C water altering thermogenesis and affecting the phenotype, we repeated our experiment using room temperature (RT) water (Fig S1D). This paradigm also induced significant increases in serum corticosterone in both ChowS and HFDS mice (Fig S1E) with the HFDS mice developing the same degree of obesity (Fig S1F) and metabolic phenotype (Fig S1I-S1K) as the cold-water induced mice (Fig 1L) without affecting overall body temperature (Fig S1G and S1H), demonstrating that the development of obesity driven by our stress protocol is unlikely to have been caused by the 10 ^{o}C water.

In order to determine the underlying cause of the altered body weight gain seen in the different treatment groups we next analysed food intake. As expected, caloric intake in the HFD mice was significantly higher than in the Chow mice (Fig 2A). Interestingly however, while ChowS mice displayed a significantly reduced *ad libitum* basal cumulative caloric intake (Fig 2B; Fig S2A), under HFDS conditions this effect was reversed (Fig 2C; Fig S2A), demonstrating that the causative effect of stress on body weight gain under high-fat-diet conditions is increased intake of the highly palatable food. Energy expenditure (EE) was significantly higher in the HFD group compared to that of the Chow group (Fig 2D) consistent with their increased energy intake and increased thermogenesis. In contrast, EE was significantly lower in the ChowS mice compared to Chow mice, again consistent with their observed lower energy intake (Fig 2E; Fig S2B). Interestingly, this stress-induced reduction in EE was also recorded in the HFDS compared to the HFD mice despite these mice consuming an increased amount of calories (Fig 2F; Fig S2B), indicating that stress can override the otherwise typical increase in EE caused by a HFD (Fig 2D; Fig S2B). The fuel source preference determined by the respiratory exchange ratio (RER) shifted towards a preferential use of fat as an energy source in the HFD compared to the Chow group (Fig 2G). Importantly, this shift was also induced by the stressor in the ChowS group (Fig 2H) and further enhanced when combined with the high caloric diet in the HFDS group (Fig 2I; Fig S2C).

The increased caloric intake due to a HFD was also associated with a strong reduction in physical activity (Fig 2J; Fig S2D). Importantly, while there was also a trend towards reduced activity in response to stress in the ChowS group (Fig 2K) this was not further exacerbated in the HFDS group (Fig 2L; Fig S2D). Investigating the influence of HFD and stress on behavioural aspects of these mice revealed some interesting alterations in their movement patterns. Plotting the preferred location of the mice in the different groups identified that ChowS mice were much less explorative than Chow or HFD mice and

they restricted themselves to a much smaller area close to the water and food hoppers (Fig 2M). Interestingly, this mobility restraining effect was less severe in the HFDS cohort (Fig 2M), supporting the concept that a highly-palatable food acts as a "comforting agent" to attenuate stress-induced anxiety behaviour (Dallman et al., 2003). Activity-categorisation of these mice further supported that HFDS mice showed a trend towards increased interaction with the hopper to take food more frequently than HFD mice, while ChowS mice showed a significantly reduced interaction with the food hopper compared to Chow mice (Fig S2E). This may also indicate that stressed-mice were attracted to consume a more palatable diet, which acted to dampen their stress-induced anxiety.

Stress alters NPY expression in the central amygdala and the arcuate nucleus

To identify the critical regions in the brain and the neuronal pathway that may be responsible for the enhancement of the obese phenotype in the HFDS mice we used a candidate gene approach. One major anxiolytic neurotransmitter known to be strongly upregulated during prolonged stress is NPY, and the amygdala is a key site for this action (Tasan et al., 2010). Importantly, NPY is also one of the strongest inducers of feeding, and these two properties combined make NPY a strong potential candidate. In the arcuate nucleus (Arc) of the hypothalamus, chronic activation of the NPY system can trigger an energy conservation state by reducing EE (Shi et al., 2013). Therefore, the dynamic changes of *Npy* expression in these two brain regions by stress might alter both behaviour and energy homeostasis. To test this, we initially employed NPY-GFP reporter mice in which GFP expression is controlled by the *Npy* promoter (van den Pol et al., 2009), and exposed them to the same stress paradigm. Body weight and fat mass in these NPY-GFP mice was affected the same way by the treatment interventions as in the WT mice (Data not shown). Brains from these mice were processed and sectioned, and NPY levels were estimated by counting the number of GFP positive (GFP+) cells in the amygdala and Arc. Under stress treatment, with and without HFD, both amygdala and Arc showed altered GFP expression compared to their corresponding diet controls, reflecting a change in the *Npy* promoter activity regulated by both diet and stress (Fig S3A). In response to stress alone in ChowS mice, more GFP+ cells were found in the lateral (LA) and basolateral amygdala (BLA) region, but not in the CeA (Fig S3A and quantified in Fig S3B and Fig S3C). Under HFD alone, there was no significant difference found in the number of GFP+ cells (Fig S3A-S3C). Strikingly, when mice were stressed in combination with HFD feeding (HFDS) GFP+ cells were significantly increased in the CeA. Interestingly, more GFP+ cells were also found in the Arc of ChowS

and HFDS mice when compared to their corresponding diet group (Fig S3E, S3F), data consistent with the observed reduction in EE in the ChowS and HFDS WT mice (Shi et al., 2013). Taken together, increased *Npy* expression in both the CeA and Arc could be the underlying mechanism that facilitates excessive feeding with reduced EE under HFDS condition.

To investigate the expression of *Npy* in neurons of the amygdala more precisely in our 4 models, translating ribosome affinity purification (TRAP) technology was used (Zhou et al., 2013; Herman et al., 2014; Allison et al., 2015; Loh et al., 2017; Farzi et al., 2018, Zhang et al., 2018). For this we crossed $Npy^{Cre/+}$ mice with conditional TRAP mice ($TRAP^{lox/lox}$) to eventually generate $Npy^{Cre/+}$;$TRAP^{lox/lox}$ mice in which the GFP-L10a ribosomal fusion protein is only produced in NPY neurons (Fig S3G and Fig S6A). These mice were then exposed to the same treatment regimens as above and the amygdala region as well as the Arc of these mice were isolated and GFP positive ribosomal complexes were purified. Using qPCR analysis, *Npy* mRNA was shown to be significantly increased in the amygdala of the ChowS mice (Fig S3H), while under HFD conditions *Npy* was significantly downregulated (HFD; Fig S3H). Interestingly, when HFD feeding was combined with the stressor, *Npy* was significantly increased compared to the HFD mice (Fig S3H). Similarly in the Arc, *Npy* was significantly higher under chronic stress in both chow (ChowS) and HFD (HFDS) condition (Fig S3H). Together this demonstrates that chronic stress activates the NPY system in both the Arc and the CeA, thereby reinforcing food consummatory behaviour and also inducing a stress-dependent energy conservation state leading to an exacerbated development of obesity.

Central amygdala NPY facilitates the development of stress-induced obesity

To determine the role of CeA NPY in the development of obesity under HFD and stress conditions in more detail, we utilised our $Npy^{lox/lox}$ mice and selectively ablated *Npy* from the CeA via bilateral injection of an AAV-Cre vector using an AAV-GFP vector as control. Injection coordinates were confirmed by injecting an AAV-FLEX-mCherry vector into a $Npy^{Cre/+}$;$TRAP^{lox/lox}$ mice showing specific expression only in the medial nuclei of the central amygdala (CeM), but not in the lateral nuclei of the central amygdala (CeL) nor in the dorsal striatal region (Fig 3A; Fig S4A). The successful deletion of *Npy* in the CeM was verified by RNAscope (Fig 3B). In addition, *in situ* hybridisation (Fig S4C) was also performed showing a significant knock down of *Npy* mRNA (Fig 3C). For *in vivo* evaluation, male $Npy^{lox/lox}$ mice injected the same way as described above were allowed to recover for 2 weeks before entering the HFDS paradigm.

These mice also showed the typical increase in corticosterone levels (Fig 3D) suggesting that *Npy* in CeA neurons is not essential for the upregulation of corticosterone. Interestingly however, CeA *Npy* ablated mice showed a significant reduction in body weight gain compared to control injected mice (Fig 3E), which also manifested itself as a significant lower absolute body weight (Fig 3F, 3G). Consistent with that, DXA analysis performed 2 weeks after the start of the HFDS paradigm revealed a significantly reduced body fat mass under the HFDS paradigm (Fig 3H) and this was due to a smaller gain of fat mass during the treatment period (Fig 3I), while no significant difference was found in lean mass, BMD or BMC (Fig 3J, 3K and 3L). The leaner phenotype in the $Npy^{lox/lox}$;AAV-Cre mice was further confirmed in individual fat deposits which showed a significant reduction in weight, both in absolute values as well as when normalised to body weight (Fig 3M; Fig S4D). Consistent with the observed increase in fat and liver weight in the control group the selective deletion of *Npy* from the CeA also caused a reduction in liver weight but had no influence on any other tissues (Fig S4E and S4F). $Npy^{lox/lox}$;AAV-Cre mice showed a significant reduction in caloric intake (Fig 3N) accompanied by reduced EE (Fig 3O), while RER was not significantly influenced (data not shown). Physical activity was significantly increased in the $Npy^{lox/lox}$;AAV-Cre mice during the onset of the dark phase but otherwise not different (Fig 3P).

To verify the results above as well as to determine the consequences of elevated NPY signalling in the CeA in the context of stress-induced obesity development, we generated a CeA specific NPY overexpression model utilising our $Npy^{Cre/+}$ knock-in line and an AAV-FLEX-NPY vector (Fig 4A). Male $Npy^{Cre/+}$ mice were bilaterally injected with the AAV-FLEX-NPY vector into the CeA. To confirm the overexpression of *Npy*, RT-qPCR was performed which demonstrated significantly higher *Npy* mRNA levels in the amygdala of the AAV-FLEX-NPY vector injected mice compared to control mice (Fig 4B). Overproduction of NPY at the protein level was also confirmed by immunohistochemistry showing strong and specific NPY staining in both the CeM neuron fibres and some synapses juxtaposing the substantia innominate (SI), internal capsule and basolateral amygdala (BLA; Fig 4C) of both brain hemispheres (H1 and H2; Fig 4C). For functional evaluation, $Npy^{Cre/+}$ mice injected with the AAV-FLEX-NPY vector were allowed to recover for 2 weeks before entering the HFDS paradigm. Importantly, NPY overproduction in the CeM led to a significant increase in body weight gain (Fig 4D) as a result of increased calorie intake (Fig 4E). Body fat mass was also significantly increased after 2 weeks of HFDS (Fig 4F) while there was no significant change in lean mass, BMD and BMC (Fig 4G, 4H, 4I and 4J), indicating that the increased feeding due to the overexpression of NPY specifically impacted fat

metabolism. NPY overproduction in the CeM did not further enhance the serum corticosterone level response to stress (Fig 4K).

NPY mediates its effects by signalling through at least 5 different Y-receptors in the mouse (Loh et al. 2015) and as such the overproduction of NPY *per se* cannot discriminate the pathway(s) activated. Importantly, NPY acting through Y1 signalling has been demonstrated to exert anxiolytic effects by antagonising the anxiogenic effect induced by corticotropin-releasing hormone (Kask et al., 2001; Sorensen et al., 2004). To gain more insights into this we repeated the overexpression experiment by employing a modified AAV-FLEX-^{Leu31,Pro34}NPY viral construct (FLEX-L/P/-NPY), known to have preference for the Y1 receptor (Lee et al., 2009). Importantly, a significant increased body weight gain was observed in mice that received the FLEX-L/P-NPY (Fig 4D), accompanied by a significantly higher fat mass after 2 weeks of HFDS treatment (Fig 4F, 4J), This increase in body fat mass was also predominantly due to increased caloric intake (Fig 4E) and no effect was seen on lean mass, BMD or BMC (Fig 4G, 4H, 4I). Interestingly, preferential activation of Y1 receptor signalling pathways resulted in significantly lower EE compared to endogenous NPY overexpression (Fig 4L, 4M). Similarly, while no differences were found in physical activity or RER between NPY overexpressing and GFP expressing mice (Fig 4N, 4P), L/P-NPY overexpressing mice showed a significantly lower RER (Fig 4Q) and a slight reduction in physical activity (Fig 4O). Serum corticosterone was again not affected by L/P-NPY overexpression (Fig 4K). Taken together, use of the ^{Leu31,Pro34}*Npy* variant suggests that Y1 receptor responsive pathways are activated by CeA derived NPY neurons during stress and contribute to the establishment of the increased obesity in the HFDS model.

Activation of NPY neurons in the CeA promotes food consumption

To further define the downstream pathways that are influenced by the activation of CeA NPY neurons we employed DREADD technology. We first injected our *Npy*$^{Cre/+}$;TRAP$^{lox/lox}$ mice with the AAV-FLEX-hM3Dq-mCherry construct bilaterally into the CeM region which expresses high level of *Npy* (Fig 5A). Successful delivery of AAV-FLEX-hM3Dq-mCherry receptors into NPY neurons was confirmed by the visualisation of red fluorescence protein (RFP) in the CeM region between the substantia innominate (SI) and internal capsule juxtaposing the basolateral amygdala (BLA) that showed complete overlap with the green fluorescence only produced by NPY neurons (Fig 5B i-iv). Importantly, no RFP-only expressing neuron cell bodies were detected, confirming the NPY neuron-specific-expression of the hM3Dq

receptor (Fig 5B v-xiii). That our injection of the AAV-FLEX-hM3Dq-mCherry receptors is highly area specific is also shown in consecutive sections spanning across the rostral to caudal CeM, but not into the CeL (Fig S4A and S4B). For functional studies, we utilised *Npy*$^{Cre/+}$ mice without the GFP reporter and visualised the expression of cFos activity as an indicator of neuronal activity using the green channel (Fig 5C). Precision of the CeM injection was confirmed by visualising RFP between substantia innominate (SI) and internal capsule (Fig 5C) and successful activation of cFos activity in the CeA is shown by the increased number of Fos-positive cells in this nuclei 1 hour after Clozapine N-oxide (CNO) treatment (Fig 5C). The CNO-induced cFos activity was also used to identify areas that may be functionally connected with CeA NPY neurons. From this analysis two main regions were identified including the Arc (Fig 5D) and the paraventricular nucleus (PVN; Fig 5E) both showing prominent increases in cFos activity in CNO-injected mice compared to saline-injected control mice. Interestingly, we found that the majority of these Fos-positive cells in the Arc resided predominantly in an area that is densely packed with NPY expressing neurons (Fig 5F), suggesting that an NPY dependent CeA circuitry may modulate Arc NPY neurons.

To verify whether NPY neurons in the CeA directly project to cells residing in the Arc and PVN we employed an AAV-FLEX construct that expresses the synaptic protein synaptophysin fused with an EGFP (EGFP-synaptophysin; AAV-FLEX-tdTomato-SynEGFP; Oh et al., 2014). Virus functionality and selectivity was confirmed by unilateral injection into the CeM of the *Npy*$^{Cre/+}$;TRAP$^{lox/lox}$ mice and subsequent visualisation of both GFP and RFP signals in the same cell in the CeM (Fig S5A). For the neuron tracing experiment, we injected the construct into the CeM of *Npy*$^{Cre/+}$ mice and verified the selectivity of the expression in the CeM and not in the CeL (Fig S5B). The EGFP-synaptophysin fusion protein was found in synapses of both RFP positive neurons and RFP negative neurons, suggesting that there are direct projections from NPY expressing neurons to surrounding non-NPY neurons in the CeA. Consistent with the cFos activation experiments, EGFP-synaptophysin labelled synapses were found in both PVN- and Arc- neurons of the CeA-injected brains but not in the control injected brains (Fig S5C and S5D).

Since both hypothalamic areas identified are known to be important in feeding and energy homeostasis regulation we performed additional functional studies to investigate the physiological consequences immediately following CeA NPY neuronal activation. For this *Npy*$^{Cre/+}$ mice injected with the stimulatory DREADD hM3Dq into the CeA and mice injected with an empty AAV control vector were allowed to recover for 14 days and then entered into our metabolic phenotyping system (Promethion) for a detailed evaluation of energy homeostatic parameters. Mice were injected with either CNO or saline at

the start of the dark phase and food intake and EE were recorded. On the next day the experiment was repeated but in the reverse order so that each mouse acted as its own control.

Importantly, food intake during the first 5 hours after CNO injection was significantly increased in the *Npy*$^{Cre/+}$;AAV-hM3Dq mice compared with the same mice treated with saline (Fig 5G). As an additional negative control we injected our *Npy*$^{Cre/+}$ mice with an AAV-empty vector to generate *Npy*$^{Cre/+}$;AAV-Empty mice. Importantly, the CNO-induced feeding response seen in the *Npy*$^{Cre/+}$;AAV-hM3Dq mice was absent in the control mice (Fig 5J). Interestingly, CNO injection into the *Npy*$^{Cre/+}$;AAV-hM3Dq mice also led to a significant reduction in EE (Fig 5H), which again was not seen in the *Npy*$^{Cre/+}$;AAV-Empty control mice (Fig 5K). Physical activity on the other hand was not altered in response to CNO in either the *Npy*$^{Cre/+}$;AAV-hM3Dq or the *Npy*$^{Cre/+}$;AAV-Empty control mice (Fig 5I, 5L). Together this suggests that activation of CeA NPY neurons drives food consummatory behaviour and at the same time prevents the normally seen activation of diet-induced EE.

To assess whether these effects on increasing food intake and reducing EE upon activation of CeA neurons actually require the presence of NPY we tested a further model. In this model we utilised our NPY-Cre knock-in mice that carry the Cre-recombinase gene instead of *Npy* under the endogenous NPY promoter, which in the homozygote state (*Npy*$^{Cre/Cre}$) represent *Npy*$^{-/-}$ mice. Importantly, CNO treatment of *Npy*$^{Cre/Cre}$;AAV-hM3Dq mice did not show any effect on food intake (Fig 5M), EE (Fig 5N) or physical activity (Fig 5O) similar to the same mice being injected with saline. These data unambiguously prove that NPY within these CeA neurons is the critical neurotransmitter that mediates the increase in food intake and the decrease in EE.

NPY deletion does not alter intrinsic excitability of CeA neurons

To test the possibility of whether deletion of *Npy* in the CeA may alter the electrical properties of these neurons we made patch clamp recordings in brain slices (Fig S4G) prepared from NPY-GFP and *Npy*$^{Cre/Cre}$-mCherry mice (Fig S4G, S4H). Comparison of NPY-GFP (n=15) and *Npy*$^{Cre/Cre}$-mCherry (n=14) recordings showed that the input resistance (340 ± 34 MΩ vs 281 ± 23 MΩ, p=0.17) and resting membrane potential (-70.00 ± 1.13 mV vs -68.02 ± 1.92, p=0.41) of these neurons did not differ in the absence of *Npy* expression. Furthermore, the active properties of neurons were also similar between genotypes, with no difference in rheobase current (66.7 ± 14.4 pA vs 47.1 ± 8.3 pA, p=0.26) or the frequency current

(F/I) relationship of action potential discharge during step current injections (Fig S4I-K). Finally, the properties of individual action potentials (AP) did not differ between recordings, with AP threshold (-38.5 ± 0.9 mV vs -37.0 ± 1.2 mV, p=0.32), AP amplitude (60.9 ± 1.6 mV vs 65.8 ± 2.4 mV, p=0.10), and AP half-width (2.19 ± 0.14 ms vs 2.31 ± 0.14 ms, p = 0.55) all similar in NPY-GFP and $Npy^{Cre/Cre}$-mCherry neurons. Thus, we conclude that the behavioural consequences of *Npy* deletion in CeA neurons cannot be explained by compensatory changes to the electrical properties of this population.

Cell type specific transcriptomic profiling of NPY neurons in the amygdala

To get a clearer insight into the nature of the NPY neurons in the amygdala we investigated their transcriptome/translational profile by employing translation ribosome affinity purification technology (TRAP) and Next-Generation RNA Sequencing. For this we utilised our $Npy^{Cre/+}$;$TRAP^{lox/lox}$ mice (Fig S6A). For RNA sequencing (RNAseq), amygdala tissue was isolated from these mice and processed via immunoprecipitation with an anti-GFP antibody for subsequent isolation of the actively translating RNA bound by the ribosomes (Fig S6B). The corresponding input samples were used as the baseline control to reflect the endogenous expression of each gene. To confirm the efficiency of our immunoprecipitation method and the specificity toward NPY neurons we first performed RT-qPCR to show that both *Npy* and GFP transcripts were significantly enriched only in the amygdala of the $Npy^{Cre/+}$;$TRAP^{lox/lox}$ mice, but not in the amygdala of the WT mice or the cerebellum of $Npy^{Cre/+}$;$TRAP^{lox/lox}$ mice where NPY is not normally expressed (Fig S6C). As an additional control, no *Npy* or GFP enrichment was found when we immunoprecipitated the tissue without the GFP antibody (Fig S6C).

RNAseq analysis of the RNA isolated from the amygdala of the $Npy^{Cre/+}$;$TRAP^{lox/lox}$ mice identified a total of 23983 genes that were mapped to the mm10 mouse reference genome (UCSC). In the immunoprecipitated (IP) sample, 4295 genes were enriched significantly with at least a 1.5 fold (or 0.58 fold with log2 scale) higher FPKM value compared to the corresponding input control (Fig S6D). A total of 2320 genes were depleted in the IP samples, indicating that these genes are not highly expressed in the NPY neurons. Volcano plot of the data revealed that the majority of the enriched genes have between 0.58 to 2 folds enrichment (Log2 scale), while a subset of 132 genes were found to be enriched over 2 fold (Log2 scale; Fig S6E; Fig S7A and S7B; Table S1). As expected, *Npy* is among one of the highest enriched genes with a 14 fold higher FPKM value compared to the input control (Fig S6F). Importantly, a group of genes which have previously been identified (Zhang et al., 2014) as marking other cell types in

the brain such as astrocytes, oligodendrocytes, microglia, endothelial cells were all deriched, and consistently, neuron-specific marker genes were significantly enriched in the IP sample compared to input control (Fig S7C). Interestingly, both *Npy1r* and *Npy5r* were significantly depleted in the IP sample, while there was no significant difference in the abundance of the *Npy2r* (Fig S6F; Fig S7D). These results are consistent with the notion that *Npy2r* are auto-receptors on NPY neurons (Shi et al, 2010), but may also have a distinct functional role in non-NPY neurons (Shi et al, 2010; Henry et al., 2015), while *Npy1r* and *Npy5r* are mostly found post-synaptically. Our results also demonstrated that these NPY neurons are GABAergic (Kim et al., 2017), with both *Gad1 (*encoding for GAD65*)* and *Gad2 (*encoding for GAD67*)* genes highly enriched in the IP samples (Fig S6F; Fig S7A). Furthermore, a number of genes that have a function in neuronal communication (*Sst, Cartpt, Cort, Nts, Ngf, Pnoc),* gene regulation (*Lhx6*) and stress response (*Crh, Crhbp*) as well as a gene, *Htr2a*, that marks orexigenic neurons (Douglass et al., 2017) were also significantly enriched (Fig S6F; Fig S7A and S7B). Importantly, *Prkcd* which is the gene encoding for PKCδ and has been linked to anorexigenic neurons in the CeA (Cai et al., 2014) was significantly reduced in NPY neurons (Fig S6F; Fig S7D), supporting the notion that NPY neurons in the CeA play a key function in promoting food intake.

Stress-induced obesity diminishes insulin inhibitory effects on CeA NPY neurons

Of the known peripheral factors that signal energy status to the brain, leptin and insulin are the most important ones. Both are known to influence NPY neurons in the hypothalamus by directly signalling through their respective receptors (Castro et al., 2013; Mendes et al., 2017; Loh et al., 2017b). However, their influence on neurons within the amygdala complex is less clear. It has been suggested that peripheral circulating hormones could also provide homeostatic feedback to the brain in extra-hypothalamic sites such as the CeA (Begg et al., 2015). Our TRAP-seq data revealed that the expression of the insulin receptor (*Insr*) is far higher than that of the leptin receptor (*Lepr*), which was not detectable in NPY neurons of the amygdala complex (Fig 6A). To further determine whether *Insr* or *Lepr* are actually co-localised with *Npy* in the CeA we employed RNAscope. Consistent with the previous finding, we found that both *Lepr* and *Insr* were co-localised with *Npy* in the Arc (Fig 6B). Interestingly, a high level of *Insr* mRNA can be found in CeA *Npy* expressing cells, while *Lepr m*RNA was completely absent from CeA NPY neurons (Fig 6C), suggesting that insulin is most likely the primary signal communicating with these NPY neurons. This is supported by results from previous work showing that

insulin infusion into the CeA downregulates *Npy* expression thereby subsequently reducing food intake (Boghossian et al., 2009; Castro et al., 2013).

To test whether stress combined with HFD also triggers such regulatory effects of insulin in the CeA NPY neurons we first measured serum insulin levels in the 4 different diet groups. While there was no major difference in basal insulin levels between the Chow and ChowS group, the HFD group showed an expected elevation of insulin (Fig 6D). Importantly, this increase was further enhanced when HFD was combined with chronic stress (Fig 6D). To further investigate whether CeA *Npy* is regulated by insulin we performed a dose-response curve and time-course experiment by injecting insulin directly into the CeA followed by RT-qPCR (Fig 6E) and found that *Npy* expression was most significantly downregulated by a dose of 5 mU of insulin 4 h after injection (Fig 6F and 6G). To also investigate the responsiveness of *Npy* expression to insulin in the CeA under chronic stress, a set of wild type mice was exposed to our stress paradigm and then injected with insulin into the CeA at the end of the study (Fig 6H). Interestingly, after insulin infusion, CeA NPY was significantly downregulated in the Chow, ChowS and HFD mice (Fig 6I). Importantly, however, insulin failed to affect *Npy* mRNA levels in the HFDS mice in which *Npy* remained highly upregulated when compared to all the other experimental groups, demonstrating that even high levels of insulin were no longer able to control these NPY neurons (Fig 6I). In addition, while baseline GTT was not different between groups (Fig 6J), this central insulin resistance phenotype was also reflected by an impaired glucose metabolism in the HFDS group compared to the HFD group with a reduced glucose clearance rate during GTT (Fig 6K). Consistent with this, after 4 weeks of the treatment, the HFDS mice still exhibited the most impaired glucose clearance rate when compared to all of the other treatment groups (Fig 6L).

Loss of *Insr* in CeA NPY neurons exacerbates stress-induced obesity

To prove more definitively that the impairment of insulin signalling in CeA NPY neurons is responsible for the food over-consummatory behaviour observed in mice under HFDS condition, we generated a new mouse model $Npy^{Cre/+};Insr^{lox/lox}$ in which the *Insr* can be deleted specifically in the CeA NPY neurons after the stereotaxic injection of 4-Hydroxytamoxifen (4-H-TAM). The successful deletion of the insulin receptor gene (*Insr)* in the CeM was verified by RNAscope (Fig. 7A) and RT-qPCR (Fig. 7B). Consistently, *Npy* expression was also significantly higher in the 4-H-TAM injected $Npy^{Cre/+};Insr^{lox/lox}$ mice than saline injected $Npy^{Cre/+};Insr^{lox/lox}$ control mice (Fig. 7C). For functional evaluation, $Npy^{Cre/+};Insr^{lox/lox}$ mice injected

with 4-H-TAM were allowed to recover for 2 weeks before entering the HFDS paradigm. Interestingly, specific deletion of *Insr* only in CeA NPY neurons also led to increased body weight gain (Fig 7D) and overall body weight (Fig 7E). Serum corticosterone was not changed (Fig 7F) which is consistent with the NPY overexpression model. Body fat mass determined by DXA was significantly increased after 2 weeks of HFDS (Fig 7G and 7H) while there were no significant changes in lean mass or BMD (Fig 7I, 7J). BMC was increased after two weeks of treatment but was not different between 4-H-TAM injected and saline injected $Npy^{Cre/+};Insr^{lox/lox}$ mice (Fig 7K). Consistent with the DXA results, and similar to the CeA NPY overexpression experiment, the weights of most of the dissected individual fat depots (i, e, m) were significantly elevated in the 4-H-TAM injected $Npy^{Cre/+};Insr^{lox/lox}$ mice (Fig 7L, S7F), while the weights of other peripheral organs were not changed (Fig S7E, S7G). Similar to *Npy* overexpression, deletion of *Insr* specifically in NPY neurons of the CeA also increased HFD consumption. Metabolic phenotyping revealed that the obese phenotype was predominantly due to a combination of increased caloric intake and decreased EE (Fig 7M and Fig 7N). RER was slightly lower (Fig 7O), while no difference was found in physical activity in the 4-H-TAM injected $Npy^{Cre/+};Insr^{lox/lox}$ mice (Fig 7P). Together our data suggest that the loss of regulatory function of insulin signalling specifically on CeA *Npy* expression is a key contributor to the accelerated obese phenotype seen under chronic stress.

DISCUSSION

Results from this study demonstrate for the first time the critical role of NPY neurons in the amygdala in controlling feeding and energy homeostasis which is especially important under conditions of stress combined with the ingestion of highly palatable food. Specifically, we identified CeA NPY neurons as the principal contributor to the increased food consummatory behaviour that promotes the development of obesity under high-stress conditions. Importantly, lack of NPY selectively in CeA neurons attenuated the obese phenotype, while overproduction of NPY in the CeA further enhanced it. Moreover, even when only a normal chow diet is provided, the acute specific activation of CeA NPY neurons by chemogenetic tools is sufficient to increase food intake and lower EE. Analysis of the transcriptomic nature of these CeA NPY neurons demonstrated that they belong to a specific subclass of neurons that have all the hallmarks for activation under stress conditions. Finally, through the use of TRAP-seq data and single cell resolution mRNA *in situ* hybridization technology we discovered for the first time that the *insr* but not the *lepr* is predominantly expressed in CeA NPY neurons, and that the loss of insulin responsiveness in these NPY neurons under HFDS condition leads to excessive NPY levels that are the primary cause for the food over-consummatory behaviour in these mice. Together, these data provide conclusive evidence that the coordinated activation of NPY neurons in the CeA and the Arc is a key driver for the exaggerated development of obesity under conditions of stress and high caloric diet consumption.

In our study, HFD combined with chronic stress facilitated both an increase in palatable food consumption and a decrease in EE as a result of the combined upregulation of NPY signalling in the CeA and Arc. In chronic stress models, stress normally reduces food intake, and in some cases body weight is also reduced correlating with the degree of stress severity (Marti et al., 1994; Rabasa et al., 2016). Interestingly, in rats forced to swim repeatedly for one hour a day, which induces hypophagia, body weight gain was not different from the control group, suggesting that compensatory mechanisms exist to restore energy balance (Rabasa et al., 2016). Similarly, although caloric intake was reduced in our ChowS mice, we found that the overall body weight gain and body fat composition were not changed, suggesting that a new homeostatic set-point was established in these mice. Our results also highlight that this restoration of energy balance is likely mediated via the activation of Arc-NPY signalling during chronic stress. We previously demonstrated that NPY derived from the Arc is critical for mediating sympathetic outflow and controlling BAT function, with chronic overexpression of NPY specifically in the Arc leading to significantly increased food intake and lower EE, establishing an energy conservation state in these mice (Shi et al., 2013). In our ChowS mice, stress also increased NPY levels in the Arc, causing

the mice to develop a condition with significantly reduced EE compared to the non-stress Chow mice. Interestingly, lowered EE was also found in our HFDS mice, contrasting to the HFD mice where over-consumption of calories led to an increase in EE in response to increased food intake, in an attempt to maintain the original homeostatic set point. Importantly, although the HFDS mice eat even more than the HFD group, they lost the ability to re-adjust their energy homeostatic system by raising EE, and instead HFDS mice develop an even lower EE set point than the Chow control mice.

The CeA is a complex forebrain structure composed of a highly interconnected network of neurons that control rewarding behaviour and fear responses (Isosaka et al., 2015). Our results now reveal that HFD combined with chronic stress significantly activate production of NPY in *Npy* expressing neurons specifically in the CeM nuclei but not the CeL subdivision (Wood et al., 2016) to also promote food intake. This is consistent with recent findings demonstrating that the CeA contains neuronal populations that are linked to anorexigenic and orexigenic output (Douglass et al., 2017; Cai et al., 2014). Specifically, a group of molecularly defined neurons that express the *Htr2a* gene has been demonstrated to modulate feeding behaviour (Douglass et al., 2017; Rossi and Stuber 2018). Molecularly, this group of cells does not overlap with an anorexigenic neuronal cell population expressing PKCδ (Cai et al., 2014; Douglass et al., 2017), but partially overlaps with other CeA markers that play a role in positive reinforcement including somatostatin (*Sst*), corticotropin-releasing hormone (*Crh*) and neurokinin B (*Tac2*). Interestingly, our TRAP-seq data also revealed that *Htr2a*, *Sst*, *Tac2 and Crh* transcripts are all, to different degrees, significantly enriched in the NPY neurons, while *Prkcd* (encoding for PKCδ) was lacking, indicating that NPY neurons overlap predominantly with the orexigenic *Hrt2a* cell population. We also demonstrated functionally for the first time that acute chemogenetic activation of CeA NPY neurons leads to a robust increase in *ad libitum* food intake which is entirely dependent on the presence of NPY. The fact that these neurons only get activated when HFD is combined with a stressor confirms the critical role of these NPY CeA neurons in mediating excessive feeding behaviour under these conditions. Our data also demonstrate for the first time that ablation of *Npy* in these CeA NPY neurons effectively attenuates the obese phenotype due to reducing feeding, while on the contrary the elevation of NPY further promotes an obese phenotype. The CeA NPY dependent development of an obese phenotype is likely mediated via NPY-Y1R signalling since chronic overexpression of the Y1R-preferring ^{Leu31,Pro34}NPY almost completely recapitulated the effect of NPY overexpression. Chronic overexpression of ^{Leu31,Pro34}NPY also triggered the establishment of a lower EE set point, indicating that activation of Y1R signalling favours the energy conserving state. However, we did not see a further exacerbation of

obesity in the ^{Leu31,Pro34}NPY overexpressing mice, suggesting that chronic activation of Y1R signalling might also activate other potential compensatory mechanisms, which presumably lead to increased fatty acid usage as the primary fuel that is reflected by the lower respiratory exchange ratio compared to AAV-NPY injected and control mice.

CeA neurons form a number of networks with other brain areas including the Arc and the PVN (Loh et al., 2017; Oh et al., 2013). Recently, it has been demonstrated that the anorexgenic regulatory effect of insulin action is mainly mediated via the NPY system, with infusion of insulin into the CeA leading to the downregulation of CeA NPY and reduced food intake (Boghossian et al., 2009; Castro et al., 2013). However, specific ablation of the insulin receptor in NPY neurons blocked this effect, mimicking a condition of insulin resistance. Lack of insulin signalling in NPY neurons in general results in higher Arc NPY levels which also subsequently leads to increased food intake and adiposity (Loh et al., 2017). Interestingly, upregulated NPY levels in the Arc caused by the loss of insulin receptor also resulted in a lower EE in these mice, which is similar to our ChowS and HFDS mice, further confirming that the fine tuning of the NPY system in the Arc is necessary for maintaining the diet-induced energy expenditure regulatory function in the body (Shi et al., 2013; Loh et al., 2017; Zhang et al., 2018).

Our chemogenetic results also provide evidence that CeA NPY derived signalling may critically influence neuronal populations in the Arc and the PVN forming the basis for a coordinated and potentially synergistic activation and enhancement from these pathways. Importantly, the activation of these neurons not only causes increased food intake but also a subsequent reduction in EE, suggesting that the NPY neurons in the CeA critically contribute to these functions. In support of this notion, CeA insulin infusion has been shown to trigger neuronal cell responses (Akt phosphorylation) in the Arc and PVN (Oh et al., 2013), indicating that the insulin-specific anorectic action is likely mediated via neurons residing in these regions (Loh et al., 2017; Boghossian et al., 2009). Taken together our results demonstrate for the first time a novel role of CeA NPY neurons, which most likely via Y1 receptor signalling control both feeding behaviour and energy homeostasis through the coordinated activation of amygdala and hypothalamic pathways, which are particularly important under conditions of stress in combination with caloric dense food.

Limitations of the study

NPY neurons in the amygdala, like anywhere else in the brain, are likely to be heterogeneous in nature co-localising with a variety of other neurotransmitters. Further analysis of the existence of such potential NPY neuronal subpopulations will be required to define whether projections to different downstream targets like the PVN, Arc or other areas in the brain are derived from different pools of amygdala NPY neurons and whether they fulfil different functions within the overall circuitry. Extending from that, while we have shown using the Y1 preferring ligand that the Y1 receptor has a prominent role in the mediation of the downstream actions from these CeA NPY neurons, further work is need to conclusively determine whether any of the other Y-receptors are also involved in the signalling.

While the different conditions of CHOW, CHOWS, HFD and HFDS clearly define different levels of NPY mRNA expression in the CeA that are linked to different levels of food intake it might be interesting to also look how this is influenced under pair-fed conditions. Finally, this study employed one specific stress paradigm that effectively induced an accelerated obese phenotype when combined with a HFD but it would also be interesting to investigate how other stressors may influence this phenotype to completely understand how the combination of stress and high caloric food may influence feeding behaviour and whole body energy homeostasis.

Acknowledgements

We thank the staff of the Garvan Institute Biological Testing Facility, staff of the Australian BioResources for taking care of our test mice. We thank the Australia genome research facility for providing us the Next-generation sequencing services and Marie Everest's technical support and Garvan molecular genetics department for genotyping the mice. This research was supported by the National Health and Medical (NHMRC) with project grant (1066809) and a Research Fellowship to HH (#1118775); Australian Research Council DP170100063 to HH and DPB.

Author contributions

C.K.I. and H.H. designed, supervised and conceptualised the study. C.K.I., A.F., I.C., R.E., Y.Q., C.D., B.G., D.S., G.G., J.K. and F.R. performed experiments and acquired the data. R.T. and G.S. designed and generated the viral vectors. J.B provided mouse models. C.D. and B.G. performed electrophysiology

experiments. C.K.I., L.Z., Y.C.S and H.H. analysed and interpreted the data. C.K.I., L.Z., A.F., R.T., N.L, D.B. and H.H. wrote, discussed and edited the manuscript.

Declaration of interests

The authors declare no competing financial interests.

Study approval

All research and animal care procedures were approved by the Garvan Institute / St. Vincent's Hospital Animal Ethics Committee and the University of New South Wales Animal Care and Ethics Committee, and the University of Newcastle Animal Care and Ethics Committee in accordance with the Australian Code of Practice for the Care and Use of Animals for Scientific Purpose.

Main figure titles and legends

Figure 1. Stress combined with high fat diet treatment exaggerates adiposity. (A) Schematic Illustration of the chronic stress phenotyping paradigm. Red dots represent 1h stress treatment. T indicates body temperature measurement done from time 0 to post-stressed 30 min. S30, stressed for 30 min, S60, stressed for 60 min, +30, 30 min after stressed. (B) Serum corticosterone levels in Chow only (Chow) or Chow combined with stress (ChowS) or High fat diet only (HFD) or HFD combined with stress (HFDS) mice at cull. (C) Representative infrared thermal image of the brown adipose tissue (BAT) and lumbar spine region of a mouse in the stress paradigm. (D, E) Temperature measured by infrared camera of (T-BAT) and lumbar (T-Back) of Chow, ChowS, HFD and HFDS mice during and after the stress paradigm. (F, G) Body weight and body weight gain of Chow, ChowS, HFD and HFDS mice starting after baseline recording at 12 weeks of age. Baseline refers to the body weight before the stress treatment while day 1 to day 12 refers to the day after the treatment has started. *** $P<0.001$ Chow vs HFD; ### $P<0.001$ HFDS vs ChowS; %%% $P<0.001$ or % $P<0.05$ HFDS vs HFD. (H) Fat mass over total tissue weight (%), (I) Lean mass, (J) Bone mass density (BMD) and (K) Bone mineral content (BMC) were monitored at both baseline and 2 weeks after treatment. (L) Weight of dissected white adipose depots, inguinal fat (i),

epididymal (e), mesenteric (m), perirenal fat (r), summed total white adipose mass and brown adipose mass (BAT). Data are means ± SEM, 8-12 mice per group, *P<0.05; **P<0.01; ***P<0.001.

Figure 2. Regulation of food intake and energy metabolism under chow and high fat diet conditions with or without chronic stress. (A-C) 24h *ad libitum* cumulative caloric intake for Chow, ChowS, HFD and HFDS mice (± SEM, 4 mice per group). (D-F) Energy expenditure, (G-I) Respiratory exchange ratio (RER) and (J-L) Physical activity (Ambulatory counts) accessed 2 weeks after the commencement of the phenotyping paradigm (± SEM, 8-12 mice per group). Shaded area from A-L indicates dark phase and un-shaded area indicates light phase. Bar graphs on the top left corner show the average 24h measurement of each group of mice. *P<0.05; **P<0.01; ***P<0.001. (M) Visualization of 24-hour footprint records of Chow, ChowS, HFD and HFDS- mice. Each dot represents the XY coordinate of the mice within the chamber. "H_2O" refers to water hopper, "F" for food hopper and "Home" for resting area. Data are represented as means ± SEM, 4 mice per group. *P<0.05; **P<0.01; ***P<0.001.

Figure 3. Ablation of *Npy* in the central amygdala attenuates stress-induced obesity. (A) Confirmation of precision of the CeA injection coordinates using an AAV-FLEX-mCherry vector in $Npy^{Cre/+}$;$TRAP^{lox/lox}$ mice. SI, substantia innominate. CeL, lateral nuclei of central amygdala. CeM, medial nuclei of central amygdala. BLA, basolateral amygdala. (B) Conformation of selective *Npy* deletion in the CeA by RNAScope. (C) Densitometry quantification of *Npy* expression in the left and right hemisphere in $Npy^{lox/lox}$;AAV-GFP control and $Npy^{lox/lox}$;AAV-Cre deletion mice by *in situ* hybridisation. (D) Serum corticosterone levels at cull under Chow, ChowS, HFD and HFDS in $Npy^{lox/lox}$;AAV-GFP control and $Npy^{lox/lox}$;AAV-Cre deletion mice. Data are means ± SEM, 4 mice per group. (E, F) Body weight gain and body weight curve of injected mice. (G) Representative image of body size after 4 week HFDS treatment. (H) DXA analysis of fat mass, (I) fat mass gain, (J) lean mass, (K) bone mass density (BMD) and (L) bone mineral content (BMC) measurement at baseline, and after 2 weeks of HFDS treatment. (M) Tissue weight of white adipose depots including inguinal fat (i), epididymal (e), mesenteric (m), perirenal fat (r) sum of total fat mass and BAT. Data are means ± SEM, 10-11 mice per group. (N) Cumulative food intake in kcal. (O) Energy expenditure and (P) Ambulatory counts after 2 weeks of HFDS treatment. Data are means ± SEM, 5 mice per group. * P<0.05; **P<0.01; ***P<0.001.

Figure 4. Overexpression of NPY and ^{Leu31,Pro34}NPY (L/P-NPY) in the central amygdala exaggerates high fat diet and stress-induced obesity. (A) Schematic of procedure and vector used. (B) Expression of CeA *Npy* (relative to *Actb* expression ± SEM, 3-4 mice per group). (C) Immunohistochemistry of NPY protein expression in the CeA. Int, internal capsule; BLA, basolateral amygdala; SI, substantia innominate; CeL, lateral nuclei of central amygdala; CeM, medial nuclei of central amygdala; H, hemisphere. (D) Body weight gain in AAV-GFP (*Npy$^{Cre/+}$*;AAV-GFP), FLEX-NPY*(Npy$^{Cre/+}$*;AAV-FLEX-NPY*)* and FLEX-L/P-NPY *(Npy$^{Cre/+}$*;AAV-FLEX-L/P-NPY) injected mice. Data are means ± SEM, 6-10 mice per group. ### P<0.001 FLEX-NPY vs AAV-GFP. ** P<0.01 FLEX-L/P-NPY vs AAV-GFP. (E) Cumulative food intake in AAV-GFP, FLEX-NPY and FLEX-L/P-NPY mice. (F) DXA analysis of fat mass, (G) lean mass, (H) bone mass density (BMD) and (I) bone mineral content (BMC) measurement at baseline and after 2 weeks of HFDS treatment. (J) Tissue weight of inguinal fat (i), epididymal (e), mesenteric (m), perirenal fat (r) and sum weight of all white adipose depots (Total). Data are means ± SEM, 6-10 mice per group. (K) Serum corticosterone levels at cull in AAV-GFP and FLEX-NPY mice under HFD condition, as well as AAV-GFP, FLEX-NPY and FLEX-L/P-NPY mice under HFDS condition. (L, M) Energy expenditure, (N, O) ambulatory counts and (P, Q) respiratory exchange ratio after 2 weeks of HFDS treatment between AAV-GFP, FLEX-NPY and FLEX-L/P-NPY mice. Data are means ± SEM, 4-6 mice per group. * P<0.05; **P<0.01; ***P<0.001.

Figure 5. Activation of NPY neurons in the central amygdala promotes food consummatory behavior. (A) Schematic of procedure and target area. CeL, lateral nuclei of central amygdala; CeM, medial nuclei of central amygdala; BLA, basolateral amygdala. (B i-iv) AAV-FLEX-hM3Dq-mCherry visualisation in the central amygdala of *Npy$^{Cre/+}$;*TRAP$^{lox/lox}$ mice. Merged image shows co-localisation of the AAV-FLEX-hM3Dq and NPY-GFP staining. (B v-viii) High magnification images of the CeM. Yellow staining represents co-localisation. (B ix-xii) Single cell level images of AAV-FLEX-hM3Dq-mCherry expressing NPY neurons. (C) Visualisation of AAV-FLEX-hM3Dq-mCherry (Red) and cFos (Green) staining in the CeM of *Npy$^{Cre/+}$*;AAV-FLEX-hM3Dq mice 1 h after CNO injection. Quantification of fos-positive hM3Dq infected NPY neurons (%). Data are means ± SEM, 3 mice per group. (D, E) Visualisation of cFos (Green) staining in the Arc and PVN of *Npy$^{Cre/+}$*;AAV-FLEX-hM3Dq mice 1h after saline or CNO injection. (F) Visualisation of DAPI (Blue), NPY (Red) and cFos (Green) staining in the Arc of *Npy$^{Cre/+}$*;AAV-FLEX-hM3Dq mice 1h after

CNO injection. Merged image shows co-localisation of DAPI, NPY and cFos staining. SI, substantia innominate; CeL, lateral nuclei of central amygdala; CeM, medial nuclei of central amygdala; BLA, basolateral amygdala; Arc, arcuate nucleus; PVN, paraventricular nucleus; 3rdV, third ventricle. (G, J, M) Cumulative food intake monitoring of the same mice injected with either CNO or saline. (H, K, N) Energy expenditure. (I, L, O) Ambulatory counts. Data are means ± SEM, 16-18 measurements per group for *Npy*$^{Cre/+}$;AAV-FLEX-hM3Dq mice. 11-13 measurements per group for *Npy*$^{Cre/+}$; Empty construct mice and 6-8 measurements per group for *Npy*$^{Cre/Cre}$; AAV-hM3Dq mice. * P<0.05; **P<0.01; ***P<0.001.

Figure 6. Loss of insulin responsiveness in CeA NPY neurons under stress and high-fat-diet condition. (A) Expression level of *Insr* and *lepr* in the immunoprecipitated (IP) mRNA of CeA NPY neurons from TRAP-seq data. FPKM, Fragment Per Kilobase of transcript per Million mapped reads. (B) RNAScope images of *Npy* and *Insr* mRNA or *Npy* and *Lepr* mRNA at single cell resolution in the arcuate nucleus (Arc). *Npy* mRNA in red and InsR and lepR in dark blue. Higher magnification images of neurons in white and black boxes. White arrow points to neurons with NPY and *Insr* coexpression, or NPY and *Lepr* coexpression. Black arrow points to neurons that only expresses *Insr,* or *Lepr* but not NPY. (C) RNAScope images of *Npy* and *Insr* mRNA or *Npy* and *Lepr* mRNA at single cell resolution in the central amygdala (CeA). *Npy* mRNA in red and InsR and lepR in dark blue. Higher magnification images of neurons in white boxed areas. White arrows point to cells with *Npy* and *Insr* coexpression, and black arrows point to neurons with *Npy* expression only. (D) Serum insulin levels of the Chow, ChowS, HFD and HFDS mice collected at the end of the treatment. Data are means ± SEM, 5-8 mice per group. (E) Schematic of procedure to test regulatory effect of insulin injection on *Npy* expression in CeA. (F) Expression of *Npy* (relative to *Actb* expression ± SEM, 4-6 mice per group) in response to stereotaxic injection of different doses of insulin in the CeA. (G) Expression of *Npy* (relative to *Actb* expression ± SEM, 4-6 mice per group) in response to stereotaxic injection of 5 mU of insulin in the CeA at different time points (relative to *Actb* expression ± SEM, 4-8 mice per group). (H) Schematic of procedure to test regulatory effect of insulin injection on *Npy* expression in CeA in Chow, ChowS, HFD and HFDS mice. (I) Expression of *Npy* relative to *Actb* expression. Data are represented as means ± SEM, 4-6 mice per group. (J-L) Glucose tolerance tests (GTT) were performed in Chow, ChowS, HFD and HFDS mice at baseline, two weeks and four weeks after the treatment, respectively. Data are means ± SEM, 5-8 mice per group. Results of the GTT were also expressed as area under the curve. * P<0.05; **P<0.01; ***P<0.001.

Figure 7. Loss of *Insr* in CeA NPY neurons exacerbated the development of stress-induced obesity. (A) Confirmation of *Insr* deletion in $Npy^{Cre/+};Insr^{lox/lox}$ mice injected with 4-Hydroxytamoxifen (4-H-TAM) or saline as control. *Npy* in red and InsR in dark blue. (B, C) Quantification of the expression of *Insr* and *Npy* mRNA in dissected CeA of $Npy^{Cre/+};Insr^{lox/lox}$ injected with 4-H-TAM or saline. Data are means ± SEM, 4-6 mice per group. (D, E) Body weight gain and body weight curve of $Npy^{Cre/+};Insr^{lox/lox(CeA\text{-}Mock\ injection)}$ and $Npy^{Cre/+};Insr^{lox/lox(CeA\text{-}4\text{-}H\text{-}TAM)}$ mice. (F) Serum corticosterone levels at cull. (G) DXA analysis of fat mass, (H) fat mass gain, (I) lean mass, (J) bone mass density (BMD) and (K) bone mineral content (BMC) measurement at baseline, and after 2 weeks of HFDS treatment. (L) Tissue weight white adipose depots including inguinal fat (i), epididymal (e), mesenteric (m), perirenal fat (r), sum of total fat mass (Total) and of BAT. (M) Cumulative food intake in kcal. (N) Energy expenditure, (O) respiratory exchange ratio and (P) ambulatory counts after 2 weeks of HFDS treatment. Data are means ± SEM, 4-7 mice per group. Boxed, dark phase. * P<0.05; **P<0.01; ***P<0.001.

STAR METHODS

CONTACT FOR REAGENT AND RESOURCE SHARING

Further information and request for resources and reagents used in this publication should be directed to Herbert Herzog (h.herzog@garvan.org.au).

EXPERIMENTAL MODEL AND SUBJECT DETAILS

Animal models and maintenance

All research and animal care procedures were approved by the Garvan Institute / St. Vincent's Hospital Animal Ethics Committee and the University of New South Wales Animal Care and Ethics Committee in accordance with the Australian Code of Practice for the Care and Use of Animals for Scientific Purpose. Mice were housed under conditions of controlled temperature (22 °C for standard laboratory temperature) and illumination (12 h light cycle, lights on at 07:00 h). Mice had free access to water and were fed either a normal chow diet (8 % calories from fat, 21 % calories from protein, 71 % calories from carbohydrate, 2.6 kcal/g; Gordon's Speciality Stock Feeds, Yanderra, NSW, Australia) before any experiments start, or high fat diet (HFD) (43 % calories from fat, 17 % calories from protein and 20 MJ/kg; Specialty Feeds, Glen Forrest, WA, Australia).

Npy$^{Cre/+}$ (Shi et al., 2013; Qi et al., 2016), NPY-GFP mice in which GFP is expressed from the *Npy* promoter (Van den Pol et al., 2009) and in house generated *Npy*$^{lox/lox}$ mice and *Npy*$^{Cre/+}$;*Insr*$^{lox/lox}$ mice (Loh et al., 2017b) were used in this study. For the ribosome translation affinity purification experiment (TRAP), ROSA26CAGGFP-L10a mice were obtained from the Jackson laboratory and crossed onto our NPY-Cre line (Zhou et al., 2013, Shi et al., 2013; Qi et al., 2016). For the phenotype experiments, mice were paired housed two weeks before the experiment began.

METHOD DETAILS

GFP positive cells counting

To access the number of GFP positive cells in different subnuclei of the amygdala and the hypothalamus, NPY-GFP mice treated with different conditions (Chow, ChowS, HFD, HFDS) for two weeks were perfused after the treatment with 4 % formaldehyde in PBS. Then perfused brains were cut at 35 µm

covering the amygdala region relative to Bregma were anterioposterior, -0.94 mm to -1.58 mm (Franklin and Paxinos, 1997). Every third section was used for counting of NPY-GFP positive neurons. Free-floating sections were mounted on Superfrost® slides (Menzel-Glaser, Braunschweig, Germany), cover slipped with fluorescence mounting medium (Dako), and photographed using DM 5500 fluorescent microscope (Leica, Germany). Eight sections from each brain were counted unilaterally from three to four different mice under blinded condition. For Arc, three sections corresponding to rostral-, medial- and caudal- region were counted from each brain, unilaterally from three different mice, also under blinded condition. Two-tailed t-test was used for statistic analysis. Statistical significance was defined as $P<0.05$.

Phenotyping paradigm for chronic stress and HFD treatment

Stress protocol used in this study has been previously used and proven to induce serum corticosterone level without affecting the body temperature (Kuo et al., 2007; Lei et al., 2014). Briefly, 10-12 weeks old WT mice were chosen based on their basal body composition by DXA analysis. Mice were treated with four conditions A) chow-fed, no stress (Chow), B) chow-fed and stress (ChowS), C) high-fat-diet fed, no stress (HFD) and D) high-fat-diet fed and stress (HFDS). For the stress protocol, mice were placed individually for 1 hour in a home cage where the bedding was replaced with 1 cm of 10 ^{o}C or room temperature water where they can freely move around. The environmental surrounding temperature was 21 ^{o}C. This procedure was repeated 3 times per week. Body temperature was monitored via infrared camera over the entire period. Body weight was recorded before the treatment starts. Basal food intake, body composition, EE, physical activity and RER were monitored before and after the 2 week treatment completes and also on the day that has no stress treatment. For HFD feeding, mice were fed from the start of the stress treatment with a high fat diet (HFD) (23 % calories from fat, 19.4 % calories from protein, 4.7 % calories from crude fiber, 4.7 % calories from acid detergent fibre and 20 MJ/Kg; Specialty Feeds, Glen Forrest, WA, Australia). At the end of the study, animals of different experimental groups were culled between 14:00 and 16:00 hour by cervical dislocation followed by decapitation and immediate serum collection. Plasma samples were stored at -20 ^{o}C until use.

Respiratory exchange ratio, physical activity, energy expenditure, food intake and behavior examination data

For phenotype characterization of our stress-induced obesity study (SIO), NPY ablation study, overexpression study, metabolic rate was measured by indirect calorimetry using an eight-chamber open-circuit calorimeter (Oxymax Series; Columbus Instruments, Columbus, OH, USA) as described previously (Zhang et al., 2010). Briefly, mice were housed individually in specially built Plexiglas cages (20.1 x 10.1 x 12.7 cm) 48 h before the actual monitoring. Temperature was maintained at 22 °C with airflow of 0.6 l/min. Mice were subsequently monitored in the system for 24 h. Oxygen consumption (VO_2) and carbon dioxide production (VCO_2) were measured every 27 min. The respiratory exchange ratio (RER) was calculated as the quotient of VCO_2/VO_2, with 100 % carbohydrate oxidation giving a value of 1, and 100 % fat oxidation giving value of 0.7 (Ferrannini, 1988, Frayn, 1983). EE (kcal heat produced) was calculated as Calorific Value (CV) x VO_2, where CV is 3.815 + 1.232 x RER (McLean and Tobin, 1987). EE was normalized to lean body mass. Data for the 24 h (from 7 am) monitoring period was averaged for 1 h intervals for EE and RER**.** Ambulatory activity of individually-housed mice was evaluated within the metabolic chambers using an OPTO-M3 sensor system (Columbus Instruments, Columbus, OH, USA), whereby ambulatory counts were a record of consecutive adjacent photo-beam breaks. Cumulative ambulatory counts of X and Y directions were recorded every minute and summed for 1 h intervals. For food intake monitoring, mice were first single-housed for 24 h, and then cumulative food intakes were either recorded manually for 72 h or monitored by the Promethion systems (Sable systems international). Food monitoring was started on the day without the stress treatment. For footprint monitoring, the Promethion system generated the coordinates corresponding to the x- and y-axis of the cage when the mice physically move each time or to interact with different objects such as the food hopper, water hopper and the home resting area. Activity categorization was determined by the software algorithm developed (Sable systems international), drinking or eating interaction was determined when there is a movement of the mice plus water or food withdrawal. Food hopper or water hopper touch was determined when there is a movement of the mice without water or food withdrawal. Entered habitat was determined when mice were rested inside the home resting area.

Stereotaxic brain injection with viral vectors

For all the stereotaxic surgery, 10-12 weeks old mice were first anestheised for surgery. Stereotaxic surgical procedure was performed using the protocol as previously described (Shi et al., 2013). To target the medial nuclei of central amygdala (CeM) brain injection coordinates relative to Bregma were anterioposterior, -1.06 mm; mediolateral, -2.6 mm; dorsoventral, -4.5 mm was chosen (Franklin and Paxinos, 1997). For all injection experiments, 0.5 µL of the viral vector was used to inject into the CeA at a rate of 0.1 µL/min using a 1 µL Hamilton Syringe and a syringe infusion pump (World Precision Instruments, Walthan, MA, USA). For *Npy* ablation study, conditional $Npy^{lox/lox}$ mice were co-injected in the central amygdala (CeA) with an AAV vector contained a cassette either expressing cre recombinase protein (AAV-Cre; 1 x 10^9 Pfu/µL) or GFP protein (AAV-GFP; 1 x 10^9 Pfu/µL), respectively. For inducible conditional $Npy^{lox/lox}$ mice, 0.45 µL of AAV-Cre vector was combined with 0.05 µL of AAV-GFP vector which were injected bilaterally into CeA while 0.05 µL of AAV-GFP vector diluted in 0.45 µL of buffer was used as control. For overexpression study, $Npy^{Cre/+}$ mice were injected with a vector containing the NPY protein coding sequence in the opposite orientation flanked by two inverted loxP sites (AAV-FLEX-NPY). Expression of *Npy* using the AAV-FLEX-*Npy* vector was activated by the presence of the cre recombinase gene only in the NPY-positive neurons causing the inversion of the NPY sequence to the active form. In the case of AAV-FLEX-*Npy* vector, 0.45 µL of the vector was also used to combine with 0.05 µL of AAV-GFP vector. To delete *Insr* in NPY neurons, 1 µL of 4-Hydroxy-tamoxifen (12 µg/µL of 60 % ethanol ; Sigma-Aldrich) was injected bilaterally into the CeA of inducible $Npy^{Cre/+};Insr^{lox/lox}$ mice while 1uL of 60 % ethanol was injected and used as mock control. After injection, all animals were kept on a heating pad during surgery and until recovery. Mice were paired housed and subsequently monitored for 2 weeks. After that, these mice were treated with our HFDS paradigm for 4 weeks as described above. Basal food intake, body composition, metabolic rate, respiratory exchange ratio and physical activity were measured and then two weeks after the HFDS treatment using the method mentioned above. Adult onset central NPY neuron-specific expression of the hM3Dq receptor in the CeA was achieved by injection of the hM3Dq-mCherry viral vector in parallel with i.c.v. 4-Hydroxytamoxifen administration in inducible $Npy^{Cre/Cre}$ and $Npy^{Cre/+}$ mice for physiology experiment. hM3Dq-mCherry viral vector was also injected into the germline transgenic $Npy^{Cre/+}$;$TRAP^{lox/lox}$ mice to confirm the co-expression between hM3Dq receptor and NPY in the CeA. Using the same CeA brain coordinates described above, 0.5 microliter of the rAAV6-hSyn-DIO-hM3Dq-mCherry vector (Addgene #44361) was used. To delete *Insr* in NPY neurons 1 uL of 4-Hydroxytamoxifen was injected bilaterally into the CeA of inducible $Npy^{Cre/+};Insr^{lox/lox}$ mice at a rate of 0.1 µl/min. To trace CeA circuits, 1 µL of AAV-phSyn1(S)-FLEX-tdTomato-T2A-SypEGFP-WPRE (Addgene #51509; 1 x 10^{11} Pfu/µL) was injected unilaterally into the CeA of germline transgenic $Npy^{Cre/+}$;$TRAP^{lox/lox}$

mice to confirm exclusive expression of the vector in CeA NPY neurons by DMI 6000 SP8 Basic Confocal (Leica). For tracing experiment the vector was then injected into the CeA of germline transgenic *Npy*$^{Cre/+}$ mice followed by immunohistochemistry using an antibody against GFP and tdTomato.

In situ hybridization

Coronal brain sections (35 µm) were cut on a cryostat and thaw-mounted on Superfrost® slides (Menzel-Glaser, Braunschweig, Germany). Matching sections from same coronal brain level were assayed together using DNA oligonucleotides complementary to mouse *Npy* (5' GAGGGTCAGTCCACACAGCCCCATTCGCTTGTTACCTAGCAT-3') as described previously (Zhang et al., 2014). Briefly, matching CeA sections of deletion and control mice were hybridised with *Npy* oligonucleotides, which were labelled with [35S] thio-dATP (Amersham Pharmacia Biotech, Buckinghamshire, UK) using terminal deoxynucleotidyltransferase (Roche, Mannheim, Germany). Silver grain densities of labelled mRNAs were analysed (Qi et al., 2016) and compared using ImageJ software (US National Institutes of Health). RNAscope duplex chromogenic assay (Advanced Cell Diagnostics, Inc.) was used to detect colocalisation of *Npy* and *Lepr*, *Insr* in the Arc and in the CeA. For this, coronal brain sections were cut and thaw-mounted on Superfrost® slides (Menzel-Glaser, Braunschweig, Germany), and double-labelled for *Npy* (ACD #313321-C2) with *Lepr* (ACD #402731) or *Npy* with *Insr* (ACD #401011) using RNAscrope® 2.5 Duplex Detection Kit following manufacturer's protocol (Advanced cell diagnostics, Inc.). Section pictures were photographed using a Zeiss Axiophot bright field light microscope

Immunohistochemistry

To confirm overexpression of NPY or ^{Leu31,Pro34}NPY in the CeA or to detect the expression of Fos positive cells in the AAV-FLEX-hM3Dq stimulated brains, immunohistochemistry using antibodies against either NPY or cFos was performed on coronal brain sections. NPY or ^{Leu31,Pro34}NPY overexpressing mice were sacrificed by cardiac perfusion with saline and 4 % formaldehyde in PBS. Brains were isolated, post-fixed at 4 °C overnight in 4 % formaldehyde in PBS and dehydrated in 30 % glucose at 4 °C until they sank. Subsequently, brains were stored at -80 °C until sectioned coronally on a cryostat at 35 µm thickness. For NPY detection, free floating sections first went through an antigen-retrieval step by incubating

sections in retrieval reagents containing 0.1 M of citric acid and 0.1 M of Tri-sodium citrate and then washed three times at room temperature (RT) for 10 min. Next, sections were blocked in 5 % normal goat serum in PBS/0.2 % Triton X for 2 h at room temperature and incubated with mouse monoclonal antibody against NPY (1:50 dilution; Sigma-Aldrich) diluents containing 5 % normal goat serum and 0.1 % BSA in PBS/0.2 % Triton X overnight at 4°C with gentle rocking. Sections were washed 3 times at RT for 10 min with PBS/0.2 % Triton and then incubated with donkey-anti-rabbit Cy3 antibody (1:250, Jackson ImmunoResearch Laboratories, Inc.) in antibody diluent for 2 h. Sections were washed 3 times as above, air-dried in dark. Finally, these sections were mounted on Superfrost® slides (Menzel-Glaser, Braunschweig, Germany), cover slipped with fluorescence mounting medium (Dako), and photographed using DM 5500 fluorescent microscope (Leica, Germany). For cFos detection, brains isolated from AAV-FLEX-hM3Dq overexpressing *Npy*$^{Cre/+}$ mice were isolated and repeated the same immunohistochemistry protocol as above but without performing the antigen-retrieval step. For primary antibody incubation, polyclonal cFos antibody (1:1200; Santa Cruz Biotechnology) was used and a donkey-anti-rabbit Alexa488 antibody (1:250, Jackson ImmunoResearch Laboratories, Inc.) was used for the secondary antibody treatment. For GFP and tdTomato amplification, polyclonal GFP (1:500; Invitrogen) and tdTomato (1:500; SICGEN) antibodies were used and a goat-anti-rabbit Alexa488 antibody (1:500; Jackson ImmunoResearch Laboratories, Inc.) and donkey-anti-goat Alexa594 antibody (1:500; Thermo Fisher Scientific) was used for the secondary antibody treatment, respectively. Slides were coverslip by Fluoroshield with DAPI (Sigma).

Amygdala isolation and translating Ribosome Affinity purification (TRAP)- RT-qPCR

TRAP experiment was performed based on the previously published protocol with some modifications (Heiman et al., 2014, Zhou et al., 2013; Loh et al., 2017). Thus, the brain was dissected out in chilled dissection buffer (1X HBSS, 2.5 mM HEPES-KOH [pH 7.4], 35 mM Glucose, and 4 mM $NaHCO_3$) supplemented with fresh 100 ug/mL of cycloheximide (Sigma). The brain was then cut twice coronally at bregma -0.82 mm and bregma -1.82 mm (Franklin and Paxinos, 2007) to expose the amygdala while the external and internal capsule and the striatum were used as the anatomical structures for reflecting on the location of the amygdala. Subsequently both amygdala were dissected out and proceeded to the TRAP experiment or snap frozen with liquid nitrogen until use. For TRAP, the dissected amygdala tissue was homogenized with a hand pestle mixer (Argos Technologies) in 500 µL of lysis buffer (20 mM HEPES

KOH [pH 7.4], 5 mM $MgCl_2$, 150 mM KCl , 0.5 mM DTT) supplemented with fresh protease inhibitor (1 tablet/mL; Roche Mini Complete, EDTA-Free), 100 µg/µL CHX and 40 U/mL of RNAsin (Promega), and then incubated at 4 °C for 5 min. Homogenates were centrifuged for 10 min at 2000 x g at 4 °C to remove pellet nuclei and cell debris, and then 50 µL of NP-40 working solution (10 %vol/vol; Biochemica) and DHPC (300 mM; Avanti Polar Lipids) were added to the supernatant and mixed gently by inverting the mixture for 10 times. After incubation on ice for 5 min, the lysate was centrifuged for 10 min at 13,000 x g. 20 % of the lysate was kept as input. Regarding the antibody-beads preparation step, 50 µL protein G Dynal magnetic beads (Invitrogen) were washed three times with 0.15 M KCl buffer (20 mM HEPES KOH [pH 7.4], 5mM $MgCl_2$, 150 mM KCl, 1 % NP-40, 0.5 mM DTT, 100 µg/ml CHX) at RT, and then 5uL of anti-GFP antibody (2 µg/µL; Invitrogen) was added into the beads and incubated with beads suspended in 0.15 M KCl buffer (275 µL) for 1h at RT with mild end-to-end rotation. Next, the antibody-bound beads were collected by using the magnetic rack and washed three times with 0.15 M KCl buffer before use. The beads were then mixed with the cell-lysate supernatant, and the mixture was incubated at 4 °C with mild end-to-end rotation overnight. Beads were subsequently collected on a magnetic rack, washed three times with 0.35 M KCl buffer (20 mM HEPES KOH [pH 7.4], 5 mM $MgCl_2$, 350 mM KCl, 1 % NP-40, 0.5mM DTT, 100 µg/ml CHX) at 4 °C, and immediately placed in 350 µL of RNA lysis buffer (RLT) supplemented with 10 % of 2-mercaptoethanol at RT and incubated for 5 min. Next, the RLT-containing RNA was purified with the RNeasy microKit (Qiagen) following manufacturer's protocol. DNase digestion step was included in the purification. RNA quantification and purity were confirmed by NanoDrop Spectrophotometers. 40 ng of RNA was used to synthesize cDNA by using the SuperScript III First-Strand Synthesis System (Thermo Fisher Scientific). RT-qPCR using primers for *Npy*, GFP was carried out in samples prior (input) and after the immunoprecipitaion in at least triplicates from 1:5 dilution of cDNA from each sample using the LightCycler® (Light-Cycler® 480 Real-Time PCR system, Roche Applied Science, Germany), SYBR Green I (Molecular Probes) and Platinum Taq DNA Polymerase (Invitrogen). Primers used for assaying *Npy*, GFP and *Actb* were previously described (Fossat et al., 2011, Shi et al., 2017). The previously described PCR condition was used in all the RT-qPCR experiments, 94 °C for 30 seconds, 62 °C for 30 seconds, 72 °C for 20 seconds for 40 cycles (Fossat et al., 2015, Ip et al., 2014). Expression of the gene was normalised to the expression of housekeeping gene *Actb* and expressed as relative to input values.

RNA isolation, quantitative real-time PCR.

CeA RNA from different animal models was extracted using an RNeasy microKit (Qiagen) following manufacturer's protocol. cDNA was synthesized from 100 ng RNA by using the SuperScript III FirstStrand Synthesis System (Thermo Fisher Scientific). The same RT-qPCR condition was used as the TRAP-RT-qPCR. Primers used for assaying *Insr* were 5'- GAGCTGTTTGAGCTGGATTA- 3' and 5'- TTCAGGATCTGAGAGTCAGT- 3'. Expression of the gene was normalised to the expression of housekeeping gene *Actb*.

RNA-sequencing and data analysis

RNA from both sides of the amygdala of *Npy*$^{Cre/+}$;TRAP$^{lox/lox}$ mice were immunoprecipitated by using the TRAP protocol described above. Input RNA and immunoprecipitated (IP) RNA from three mice were pooled together to give enough material for RNA-sequencing. Two replicates were included for both IP and input samples. A total of 200 ng of the IP RNA and its corresponding input control was used for RNA-sequencing experiment. Illumina HiSeq HT chemistry sequencing with 100 base pair single-end read was employed. RNA quality and quantity were determined by Bioanalyzer Nanokit (Agilent). The same amount of RNA from both the immunoprecipitated samples and the input samples were used for library preparation (Illumina) in the Australian Genome Research Facility. Sequencing quality check of the raw sequencing reads was performed using the FastQC tool (Andrew S. 2010) through the Galaxy Project platform. No over-represented sequences were detected, indicating that adapter sequences did not affect the overall dataset. Read alignment was performed using TopHat (Trapnell et al., 2012) with default parameter, and iGenome (http://cole-trapnell-lab.github.io/cufflinks//igenome_table/index.html) mm10 UCSC transcriptome annotation. Differential expression was determined by Cufflinks and Cuffdiff analysis, and a false discovery rate of <0.05 were considered to be statistically significant. All RNAseq data have been deposited into NCBI's GRP with accession number GSE128413.

Glucose tolerance tests, Insulin and corticosterone measurement

Glucose tolerance tests (GTT) were performed at the end of the two weeks and four weeks of the experimental paradigm. Mice from different groups (Chow, ChowS, HFD and HFDS) were first fasted for 6h and then they were administered i.p. with glucose (1 g/kg body weight). Blood glucose levels were assessed at 0, 15, 30, 60, and 90 min after glucose administration using a Accu-chek Go glucometer

(Roche, Dee Why, Australia). For insulin detection, serum of the mice collected from the end of the study were measured using insulin RIA kits (Millipore). Corticosterone measurements were performed by using a Corticosterone Double Antibody RIA kit from MP Biomedicals (MP Biomedicals, LLC, Orangeburg, NY, USA).

Central amygdala insulin infusion and RT-qPCR

To test for the dose-dependent effect of insulin on CeA NPY expression, mice were first anesthetized and placed on a Kopf stereotaxic frame (David Kopf Instruments, Tujunga, CA, USA). Subsequently, 1 mU, 5 mU or 10 mU of insulin were stereotaxically injected into the CeA at a rate of 0.1 ml/min using a 1 µl Hamilton Syringe and a syringe infusion pump (World Precision Instruments, Walthan, MA, USA) and then the CeA was dissected after 4 h under the inverted microscope for quantitative real-time PCR (RT-qPCR) to assay for *Npy* mRNA expression. For time-dependent effect of insulin, 5 mU of insulin was injected into the CeA and then the CeA was dissected after 1 h, 4 h and 6 h. To test for the responsiveness of CeA to insulin under Chow, ChowS, HFD and HFDS treatment, mice went through these paradigms were injected with 5 mU of insulin and the CeA was dissected after 4 h for RT-qPCR. Brain injection coordinates relative to Bregma were anterioposterior, -1.06 mm; mediolateral, -2.6 mm; dorsoventral, -4.5 mm, corresponding to the central amygdala (Franklin and Paxinos, 1997).

Body temperature measurement with Infrared Imaging

Measurement of whole body temperature and brown adipose tissue temperatures was performed by infrared imagine as previously described (Farzi et al., 2018). Skin temperature at the interscapular brown adipose tissue (BAT) as well as the lumbar spine region measured for Chow, ChowS, Chow RT. S, HFD, HFDS and HFD RT. S mice at baseline and at the end of the experiment after 2 weeks by non-invasive high-sensitivity infrared imaging with a high-sensitivity infrared camera (ThermoCAM T640, FLIR, Danderyd, Sweden, sensitivity = 0.04˚C). On the day of measurement, all mice were singly housed and acclimatized for 2 h before the experiment. In order to gain insight of the impact of the stress treatment on mice, body temperature was measured at baseline 0 h then 30 min and 1 h during the stress paradigm as well as 30 min after the stress.

Electrophysiology

Brain slices were prepared from NPY-GFP and *Npy*$^{lox/lox}$-mCherry mice similar to previously described methods (Hunt et al., 2017; Yeoh et al., 2018). Briefly, mice were anesthetized using Ketamine (100mg/kg), decapitated, and brains were removed while submerged in ice-cold sucrose-substituted ACSF containing (in mM): 250 sucrose, 25 $NaHCO_3$, 10 glucose, 2.5 KCl, 1 NaH_2PO_4, 1 $MgCl_2$ and 2.5 $CaCl_2$. Coronal brain slices (250 μm thick) were prepared using a vibratome (7000 SMZ, Campden Instruments) and subsequently stored in an interface chamber containing ACSF (118 mM substituted for sucrose). This tissue was maintained at room temperature (22-24 °C) and allowed to equilibrate for 1 h prior to recording.

Following equilibration, slices were individually transferred to a recording chamber, continually superfused (bath volume 0.4 mls; exchange rate 4–6 bath volumes/min) with ACSF bubbled with Carbanox (95 % O2 and 5 % CO2) to achieve a pH of 7.3–7.4. Recordings were obtained at room temperature (21–24 °C) and neurons were visualized using a Scientifica SliceScope with near-infrared differential interference contrast optics connected at a camera (Jenoptik ProgRes MF cool). Recordings focussed on the medial division of the CeM where GFP-, or mCherry-expressing neurons were targeted. Patch pipettes (4-8 MΩ) were filled with a potassium gluconate-based internal solution containing (in mM): 135 $C_6H_{11}KO_7$, 6 NaCl, 2 $MgCl_2$, 10 HEPES, 0.1 EGTA, 2 MgATP, 0.3 NaGTP, pH 7.3 (with KOH). All whole-cell recordings were first established in voltage-clamp (holding potential -70 mV). Data were amplified using a Multiclamp 700B amplifier (Molecular Devices) digitized online (sampled at 20 kHz and filtered at 10 kHz) via an ITC-18 computer interface (Instrutech), acquired and stored using Axograph X software (Axograph X). After obtaining the whole-cell recording configuration, series resistance (<30 MΩ) and input resistance were calculated based on the response to a hyperpolarising voltage step (5 mV , 10 ms). AP discharge properties were studied by injecting a series of depolarizing step-currents (20 pA increments, 900 ms duration, delivered every 8 seconds) through the recording electrode. During this protocol voltage deflections were limited, to avoid cell damage, by terminating the protocol if sustained depolarizations exceeded - 20 mV (i.e., in parts of the voltage trace not containing APs).

Statistical analyses

All data are expressed as means ± SEM. For energy expenditure (EE), physical activity and RER it was monitored over the continuous 24-h period (07:00-07:00) and were averaged for the whole 24-h period, as well as for the light and dark periods. For body weight and body weight gain it was monitored over the course of the treatments. Differences between different treatments and genotypes were assessed by two way ANOVA or repeated-measures ANOVA. Statistical analyses were performed in GraphPad Prism. For cumulative food intake, fat mass, lean mass, BMD and BMC, dissected tissue weight, two-tailed t-test was used. Statistical significance was defined as $P<0.05$.

SUPPLEMENTAL TABLE

Supplementary Table 1. Extended data from Supplementary figure 6. Differentially expressed genes in the amygdala between Input RNA and IP RNA of *Npy*$^{Cre/+}$;TRAP$^{lox/lox}$ mice.

REFERENCES

Andrews S. (2010). FastQC: a quality control tool for high throughput sequence data. Available online at:http://www.bioinformatics.babraham.ac.uk/projects/fastqc

ALLISON, M. B., PATTERSON, C. M., KRASHES, M. J., LOWELL, B. B., MYERS, M. G., JR. & OLSON, D. P. 2015. TRAP-seq defines markers for novel populations of hypothalamic and brainstem LepRb neurons. *Mol Metab,* 4**,** 299-309.

ARMARIO, A. 2006. The hypothalamic-pituitary-adrenal axis: what can it tell us about stressors? *CNS Neurol Disord Drug Targets,* 5**,** 485-501.

BALDOCK, P. A., LIN, S., ZHANG, L., KARL, T., SHI, Y., DRIESSLER, F., ZENGIN, A., HORMER, B., LEE, N. J., WONG, I. P., LIN, E. J., ENRIQUEZ, R. F., STEHRER, B., DURING, M. J., YULYANINGSIH, E., ZOLOTUKHIN, S., RUOHONEN, S. T., SAVONTAUS, E., SAINSBURY, A. & HERZOG, H. 2014. Neuropeptide y attenuates stress-induced bone loss through suppression of noradrenaline circuits. *J Bone Miner Res,* 29**,** 2238-49.

BEGG, D. P., MAY, A. A., MUL, J. D., LIU, M., D'ALESSIO, D. A., SEELEY, R. J. & WOODS, S. C. 2015. Insulin Detemir Is Transported From Blood to Cerebrospinal Fluid and Has Prolonged Central Anorectic Action Relative to NPH Insulin. *Diabetes,* 64**,** 2457-66.

BOGHOSSIAN, S., LEMMON, K., PARK, M. & YORK, D. A. 2009. High-fat diets induce a rapid loss of the insulin anorectic response in the amygdala. *Am J Physiol Regul Integr Comp Physiol,* 297**,** R1302-11.

BRUNING, J. C., GAUTAM, D., BURKS, D. J., GILLETTE, J., SCHUBERT, M., ORBAN, P. C., KLEIN, R., KRONE, W., MULLER-WIELAND, D. & KAHN, C. R. 2000. Role of brain insulin receptor in control of body weight and reproduction. *Science,* 289**,** 2122-5.

CAI, H., HAUBENSAK, W., ANTHONY, T. E. & ANDERSON, D. J. 2014. Central amygdala PKC-delta(+) neurons mediate the influence of multiple anorexigenic signals. *Nat Neurosci,* 17**,** 1240-8.

CASTRO, G., MF, C. A., WEISSMANN, L., QUARESMA, P. G., KATASHIMA, C. K., SAAD, M. J. & PRADA, P. O. 2013. Diet-induced obesity induces endoplasmic reticulum stress and insulin resistance in the amygdala of rats. *FEBS Open Bio,* 3**,** 443-9.

CAVAGNINI, F., CROCI, M., PUTIGNANO, P., PETRONI, M. L. & INVITTI, C. 2000. Glucocorticoids and neuroendocrine function. *Int J Obes Relat Metab Disord,* 24 Suppl 2**,** S77-9.

DALLMAN, M. F., PECORARO, N., AKANA, S. F., LA FLEUR, S. E., GOMEZ, F., HOUSHYAR, H., BELL, M. E., BHATNAGAR, S., LAUGERO, K. D. & MANALO, S. 2003. Chronic stress and obesity: a new view of "comfort food". *Proc Natl Acad Sci U S A,* 100**,** 11696-701.

DALLMAN, M. F., PECORARO, N. C. & LA FLEUR, S. E. 2005. Chronic stress and comfort foods: self-medication and abdominal obesity. *Brain Behav Immun,* 19**,** 275-80.

DALLMAN, M. F., STRACK, A. M., AKANA, S. F., BRADBURY, M. J., HANSON, E. S., SCRIBNER, K. A. & SMITH, M. 1993. Feast and famine: critical role of glucocorticoids with insulin in daily energy flow. *Front Neuroendocrinol,* 14**,** 303-47.

DOUGLASS, A. M., KUCUKDERELI, H., PONSERRE, M., MARKOVIC, M., GRUNDEMANN, J., STROBEL, C., ALCALA MORALES, P. L., CONZELMANN, K. K., LUTHI, A. & KLEIN, R. 2017. Central amygdala circuits modulate food consumption through a positive-valence mechanism. *Nat Neurosci,* 20**,** 1384-1394.

EPEL, E., JIMENEZ, S., BROWNELL, K., STROUD, L., STONEY, C. & NIAURA, R. 2004. Are stress eaters at risk for the metabolic syndrome? *Ann N Y Acad Sci,* 1032**,** 208-10.

FARZI, A., LAU, J., IP, C. K., QI, Y., SHI, Y. C., ZHANG, L., TASAN, R., SPERK, G. & HERZOG, H. 2018. Arcuate

nucleus and lateral hypothalamic CART neurons in the mouse brain exert opposing effects on energy expenditure. *Elife,* 7.

FERRANNINI, E. 1988. The theoretical bases of indirect calorimetry: a review. *Metabolism,* 37**,** 287-301.

FOSSAT, N., IP, C. K., JONES, V. J., STUDDERT, J. B., KHOO, P. L., LEWIS, S. L., POWER, M., TOURLE, K., LOEBEL, D. A., KWAN, K. M., BEHRINGER, R. R. & TAM, P. P. 2015. Context-specific function of the LIM homeobox 1 transcription factor in head formation of the mouse embryo. *Development,* 142**,** 2069-79.

FRAYN, K. N. 1983. Calculation of substrate oxidation rates in vivo from gaseous exchange. *J Appl Physiol Respir Environ Exerc Physiol,* 55**,** 628-34.

HAN, W., TELLEZ, L. A., RANGEL, M. J., JR., MOTTA, S. C., ZHANG, X., PEREZ, I. O., CANTERAS, N. S., SHAMMAH-LAGNADO, S. J., VAN DEN POL, A. N. & DE ARAUJO, I. E. 2017. Integrated Control of Predatory Hunting by the Central Nucleus of the Amygdala. *Cell,* 168**,** 311-324 e18.

HEILIG, M. 2004. The NPY system in stress, anxiety and depression. *Neuropeptides,* 38**,** 213-24.

HEIMAN, M., KULICKE, R., FENSTER, R. J., GREENGARD, P. & HEINTZ, N. 2014. Cell type-specific mRNA purification by translating ribosome affinity purification (TRAP). *Nat Protoc,* 9**,** 1282-91.

HUNT, S., SUN, Y., KUCKDERELI, H., KLEIN, R and SAH, P. 2017. Intrinsic Circuits in the Lateral Central Amygdala. Hunt, S., Sun, Y., Kucukdereli, H., Klein, R., & Sah, P. (2017). Intrinsic Circuits in the Lateral Central Amygdala. *eNeuro*, 4(1), ENEURO.0367-16.2017.

IP, C. K., FOSSAT, N., JONES, V., LAMONERIE, T. & TAM, P. P. 2014. Head formation: OTX2 regulates Dkk1 and Lhx1 activity in the anterior mesendoderm. *Development,* 141**,** 3859-67.

ISOSAKA, T., MATSUO, T., YAMAGUCHI, T., FUNABIKI, K., NAKANISHI, S., KOBAYAKAWA, R. & KOBAYAKAWA, K. 2015. Htr2a-Expressing Cells in the Central Amygdala Control the Hierarchy between Innate and Learned Fear. *Cell,* 163**,** 1153-1164.

KASK, A., NGUYEN, H. P., PABST, R. & VON HORSTEN, S. 2001. Neuropeptide Y Y1 receptor-mediated anxiolysis in the dorsocaudal lateral septum: functional antagonism of corticotropin-releasing hormone-induced anxiety. *Neuroscience,* 104**,** 799-806.

KIM, H., WHANG, W. W., KIM, H. T., PYUN, K. H., CHO, S. Y., HAHM, D. H., LEE, H. J. & SHIM, I. 2003. Expression of neuropeptide Y and cholecystokinin in the rat brain by chronic mild stress. *Brain Res,* 983**,** 201-8.

KIM, J., ZHANG, X., MURALIDHAR, S., LEBLANC, S. A. & TONEGAWA, S. 2017. Basolateral to Central Amygdala Neural Circuits for Appetitive Behaviors. *Neuron,* 93**,** 1464-1479 e5.

KUO, L. E., KITLINSKA, J. B., TILAN, J. U., LI, L., BAKER, S. B., JOHNSON, M. D., LEE, E. W., BURNETT, M. S., FRICKE, S. T., KVETNANSKY, R., HERZOG, H. & ZUKOWSKA, Z. 2007. Neuropeptide Y acts directly in the periphery on fat tissue and mediates stress-induced obesity and metabolic syndrome. *Nat Med,* 13**,** 803-11.

LEE, N. J. & HERZOG, H. 2009. NPY regulation of bone remodelling. *Neuropeptides,* 43**,** 457-63.

LEVINE, A. S. & MORLEY, J. E. 1981. Stress-induced eating in rats. *Am J Physiol,* 241**,** R72-6.

LOH, K., HERZOG, H. & SHI, Y. C. 2015. Regulation of energy homeostasis by the NPY system. *Trends Endocrinol Metab,* 26**,** 125-35.

LOH, K., SHI, Y. C., WALTERS, S., BENSELLAM, M., LEE, K., DEZAKI, K., NAKATA, M., IP, C. K., CHAN, J. Y., GURZOV, E. N., THOMAS, H. E., WAIBEL, M., CANTLEY, J., KAY, T. W., YADA, T., LAYBUTT, D. R., GREY, S. T. & HERZOG, H. 2017. Inhibition of Y1 receptor signaling improves islet transplant outcome. *Nat Commun,* 8**,** 490.

LOH, K., ZHANG, L., BRANDON, A., WANG, Q., BEGG, D., QI, Y., FU, M., KULKARNI, R., TEO, J., BALDOCK, P., BRUNING, J. C., COONEY, G., NEELY, G. & HERZOG, H. 2017b. Insulin controls food intake and energy balance via NPY neurons. *Mol Metab,* 6**,** 574-584.

MARTI, O., MARTI, J. & ARMARIO, A. 1994. Effects of chronic stress on food intake in rats: influence of

stressor intensity and duration of daily exposure. *Physiol Behav,* 55**,** 747-53.

MCEWEN, B. S. 2004. Protection and damage from acute and chronic stress: allostasis and allostatic overload and relevance to the pathophysiology of psychiatric disorders. *Ann N Y Acad Sci,* 1032**,** 1-7.

MCLEAN, J. A., TOBIN, G. 1987. Animal and human calorimetry. *New York: Cambridge University Press*.

MENDES, N. F., CASTRO, G., GUADAGNINI, D., TOBAR, N., COGNUCK, S. Q., ELIAS, L. L., BOER, P. A. & PRADA, P. O. 2017. Knocking down amygdalar PTP1B in diet-induced obese rats improves insulin signaling/action, decreases adiposity and may alter anxiety behavior. *Metabolism,* 70**,** 1-11.

MORLEY, J. E., LEVINE, A. S. & ROWLAND, N. E. 1983. Minireview. Stress induced eating. *Life Sci,* 32**,** 2169-82.

OH, H., BOGHOSSIAN, S., YORK, D. A. & PARK-YORK, M. 2013. The effect of high fat diet and saturated fatty acids on insulin signaling in the amygdala and hypothalamus of rats. *Brain Res,* 1537**,** 191-200.

OH, S. W., HARRIS, J. A., NG, L., WINSLOW, B., CAIN, N., MIHALAS, S., WANG, Q., LAU, C., KUAN, L., HENRY, A. M., MORTRUD, M. T., OUELLETTE, B., NGUYEN, T. N., SORENSEN, S. A., SLAUGHTERBECK, C. R., WAKEMAN, W., LI, Y., FENG, D., HO, A., NICHOLAS, E., HIROKAWA, K. E., BOHN, P., JOINES, K. M., PENG, H., HAWRYLYCZ, M. J., PHILLIPS, J. W., HOHMANN, J. G., WOHNOUTKA, P., GERFEN, C. R., KOCH, C., BERNARD, A., DANG, C., JONES, A. R. & ZENG, H. 2014. A mesoscale connectome of the mouse brain. *Nature,* 508**,** 207-14.

PRIMEAUX, S. D., YORK, D. A. & BRAY, G. A. 2006. Neuropeptide Y administration into the amygdala alters high fat food intake. *Peptides,* 27**,** 1644-51.

QI, Y., FU, M. & HERZOG, H. 2016. Y2 receptor signalling in NPY neurons controls bone formation and fasting induced feeding but not spontaneous feeding. *Neuropeptides,* 55**,** 91-7.

RABASA, C., WINSA-JORNULF, J., VOGEL, H., BABAEI, C. S., ASKEVIK, K. & DICKSON, S. L. 2016. Behavioral consequences of exposure to a high fat diet during the post-weaning period in rats. *Horm Behav,* 85**,** 56-66.

RASMUSSON, A. M., HAUGER, R. L., MORGAN, C. A., BREMNER, J. D., CHARNEY, D. S. & SOUTHWICK, S. M. 2000. Low baseline and yohimbine-stimulated plasma neuropeptide Y (NPY) levels in combat-related PTSD. *Biol Psychiatry,* 47**,** 526-39.

ROSSI, M. A. & STUBER, G. D. 2018. Overlapping Brain Circuits for Homeostatic and Hedonic Feeding. *Cell Metab,* 27**,** 42-56.

SHI, Y. C., IP, C. K., REED, F., SARRUF, D. A., WULFF, B. S. & HERZOG, H. 2017. Y5 receptor signalling counteracts the anorectic effects of PYY3-36 in diet-induced obese mice. *J Neuroendocrinol,* 29.

SHI, Y. C., LAU, J., LIN, Z., ZHANG, H., ZHAI, L., SPERK, G., HEILBRONN, R., MIETZSCH, M., WEGER, S., HUANG, X. F., ENRIQUEZ, R. F., BALDOCK, P. A., ZHANG, L., SAINSBURY, A., HERZOG, H. & LIN, S. 2013. Arcuate NPY controls sympathetic output and BAT function via a relay of tyrosine hydroxylase neurons in the PVN. *Cell Metab,* 17**,** 236-48.

SORENSEN, G., LINDBERG, C., WORTWEIN, G., BOLWIG, T. G. & WOLDBYE, D. P. 2004. Differential roles for neuropeptide Y Y1 and Y5 receptors in anxiety and sedation. *J Neurosci Res,* 77**,** 723-9.

STONE, A. A. & BROWNELL, K. D. 1994. The stress-eating paradox: Multiple daily measurements in adult males and females. *Psychology & Health,* 9**,** 425-436.

TASAN, R. O., NGUYEN, N. K., WEGER, S., SARTORI, S. B., SINGEWALD, N., HEILBRONN, R., HERZOG, H. & SPERK, G. 2010. The central and basolateral amygdala are critical sites of neuropeptide Y/Y2 receptor-mediated regulation of anxiety and depression. *J Neurosci,* 30**,** 6282-90.

TRAPNELL, C., ROBERTS, A., GOFF, L., PERTEA, G., KIM, D., KELLEY, D. R., PIMENTEL, H., SALZBERG, S. L., RINN, J. L. & PACHTER, L. 2012. Differential gene and transcript expression analysis of RNA-seq experiments with TopHat and Cufflinks. *Nat Protoc,* 7**,** 562-78.

VAN DEN POL, A. N., YAO, Y., FU, L. Y., FOO, K., HUANG, H., COPPARI, R., LOWELL, B. B. & BROBERGER, C. 2009. Neuromedin B and gastrin-releasing peptide excite arcuate nucleus neuropeptide Y neurons in a novel transgenic mouse expressing strong Renilla green fluorescent protein in NPY neurons. *J Neurosci,* 29**,** 4622-39.

WOOD, J., VERMA, D., LACH, G., BONAVENTURE, P., HERZOG, H., SPERK, G. & TASAN, R. O. 2016. Structure and function of the amygdaloid NPY system: NPY Y2 receptors regulate excitatory and inhibitory synaptic transmission in the centromedial amygdala. *Brain Struct Funct,* 221**,** 3373-91.

YEHUDA, R., BRAND, S. & YANG, R. K. 2006. Plasma neuropeptide Y concentrations in combat exposed veterans: relationship to trauma exposure, recovery from PTSD, and coping. *Biol Psychiatry,* 59**,** 660-3.

YEOH, JW., JAMES, MH., ADAMS, CD., BAINS, JS., SAKURI, T., ASTON-JONES, G., GRAHAM, BA. & DAYAS, CD. 2018. Activation of lateral hypothalamic group III metabotropic glutamate receptors suppresses cocaine-seeking following abstinence and normalizes drug-associated increases in excitatory drive to orexin/hypocretin cells. *Neuropharmacology, In Press, https://doi.org/10.1016/j.neuropharm.2018.09.033*

ZAKRZEWSKA, K. E., CUSIN, I., STRICKER-KRONGRAD, A., BOSS, O., RICQUIER, D., JEANRENAUD, B. & ROHNER-JEANRENAUD, F. 1999. Induction of obesity and hyperleptinemia by central glucocorticoid infusion in the rat. *Diabetes,* 48**,** 365-70.

ZHANG, L., IP, C. K., LEE, I. J., QI, Y., REED, F., KARL, T., LOW, J. K., ENRIQUEZ, R. F., LEE, N. J., BALDOCK, P. A. & HERZOG, H. 2018. Diet-induced adaptive thermogenesis requires neuropeptide FF receptor-2 signalling. *Nat Commun,* 9**,** 4722.

ZHANG, L., LEE, I. C., ENRIQUEZ, R. F., LAU, J., VAHATALO, L. H., BALDOCK, P. A., SAVONTAUS, E. & HERZOG, H. 2014. Stress- and diet-induced fat gain is controlled by NPY in catecholaminergic neurons. *Mol Metab,* 3**,** 581-91.

ZHANG, L., MACIA, L., TURNER, N., ENRIQUEZ, R. F., RIEPLER, S. J., NGUYEN, A. D., LIN, S., LEE, N. J., SHI, Y. C., YULYANINGSIH, E., SLACK, K., BALDOCK, P. A., HERZOG, H. & SAINSBURY, A. 2010. Peripheral neuropeptide Y Y1 receptors regulate lipid oxidation and fat accretion. *Int J Obes (Lond),* 34**,** 357-73.

ZHOU, P., ZHANG, Y., MA, Q., GU, F., DAY, D. S., HE, A., ZHOU, B., LI, J., STEVENS, S. M., ROMO, D. & PU, W. T. 2013. Interrogating translational efficiency and lineage-specific transcriptomes using ribosome affinity purification. *Proc Natl Acad Sci U S A,* 110**,** 15395-400.

Figure 1

Click here to access/download;Figure;Figure 1.jpg

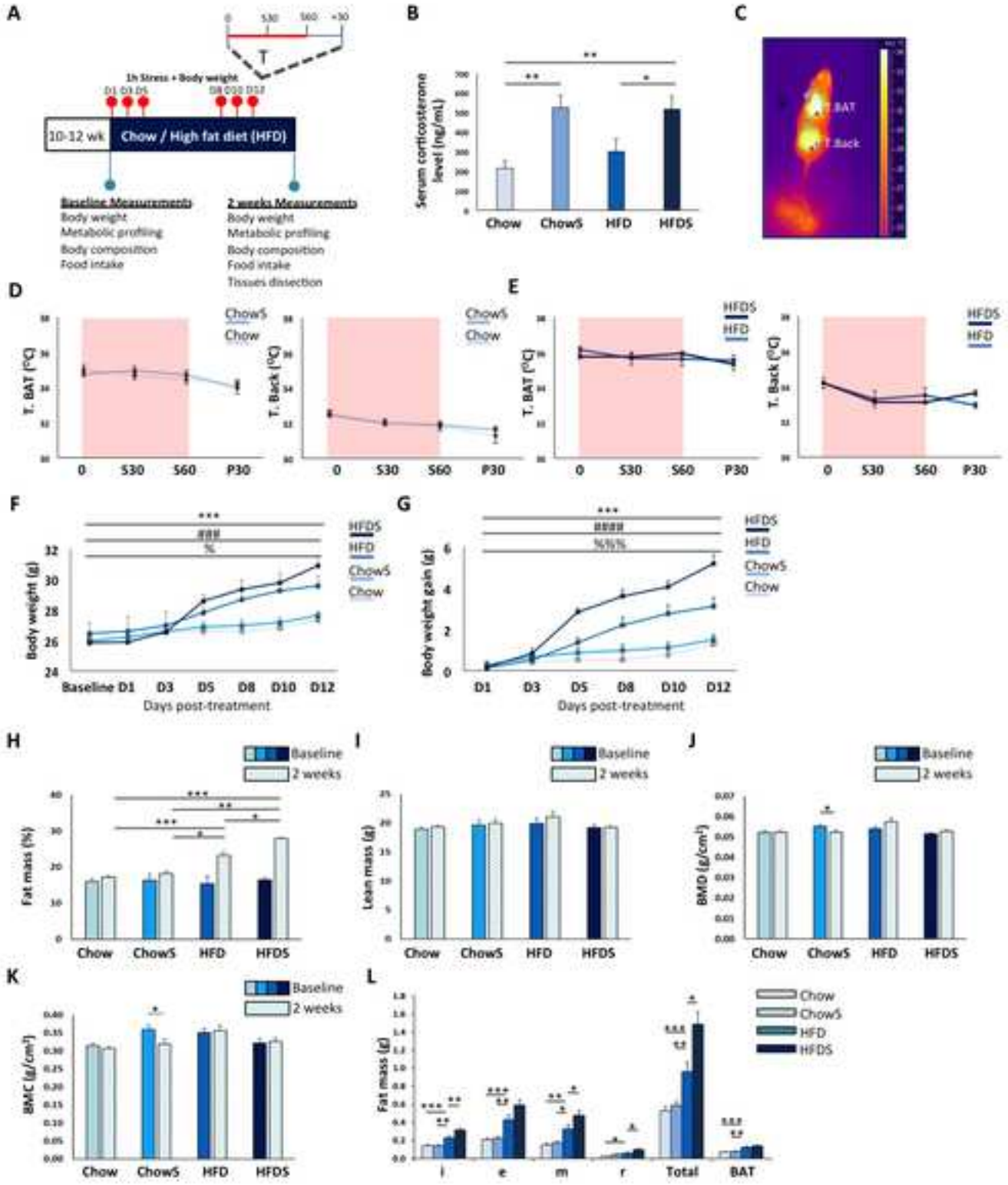

Figure 2

Click here to access/download;Figure;Figure 2.jpg

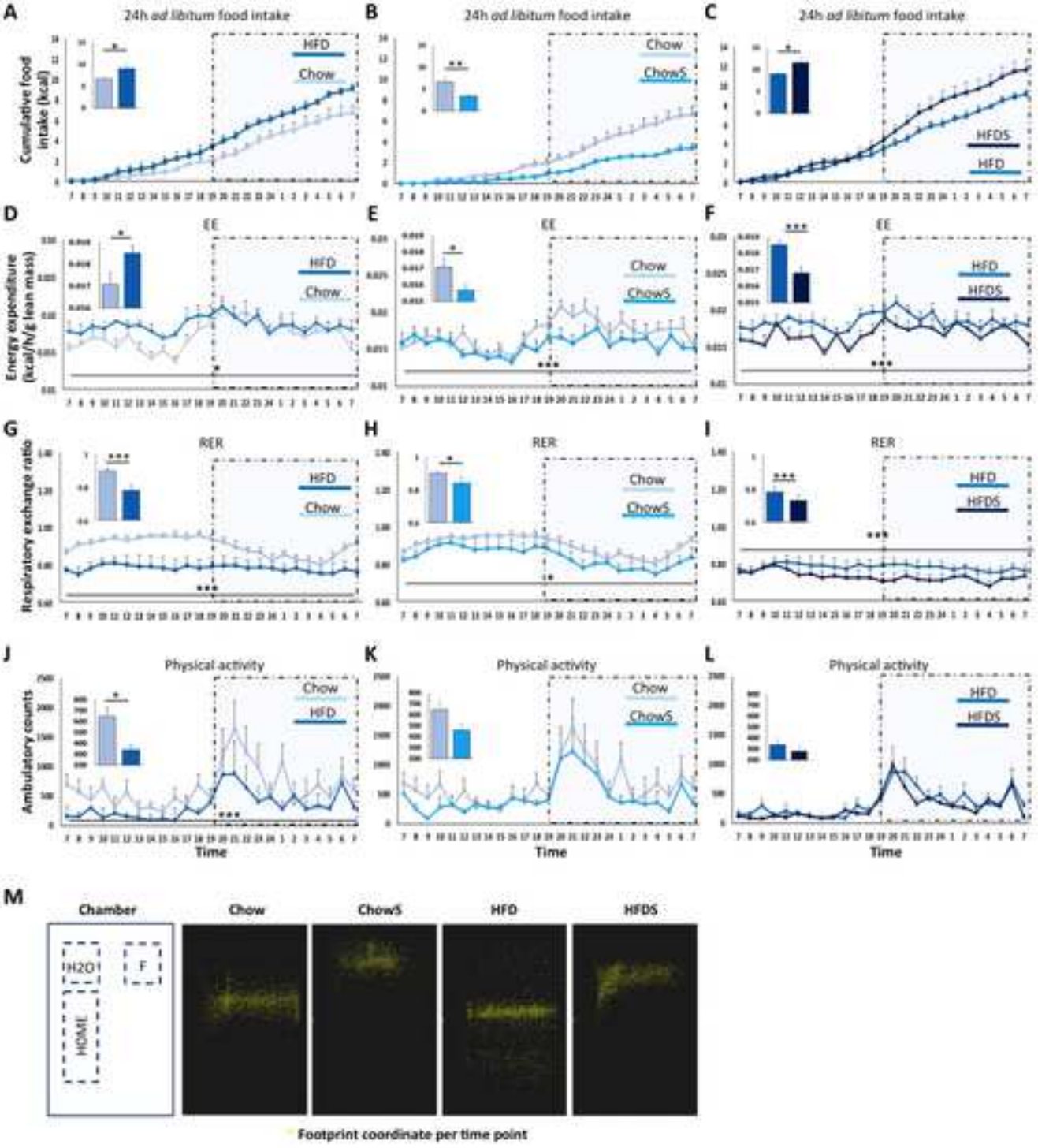

Figure 3

Click here to access/download;Figure;Figure 3.jpg

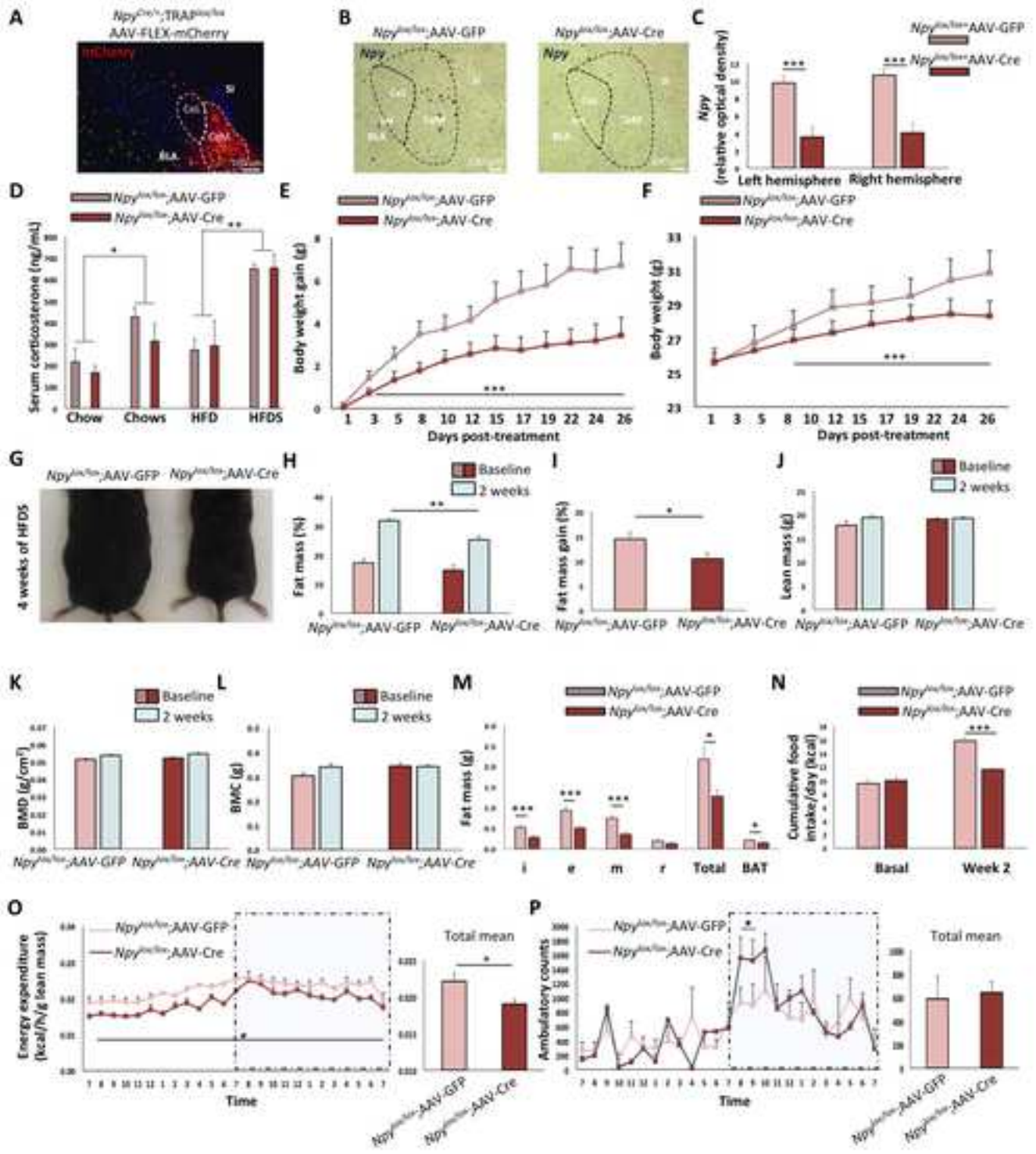

Figure 4

Click here to access/download;Figure;Figure 4.jpg

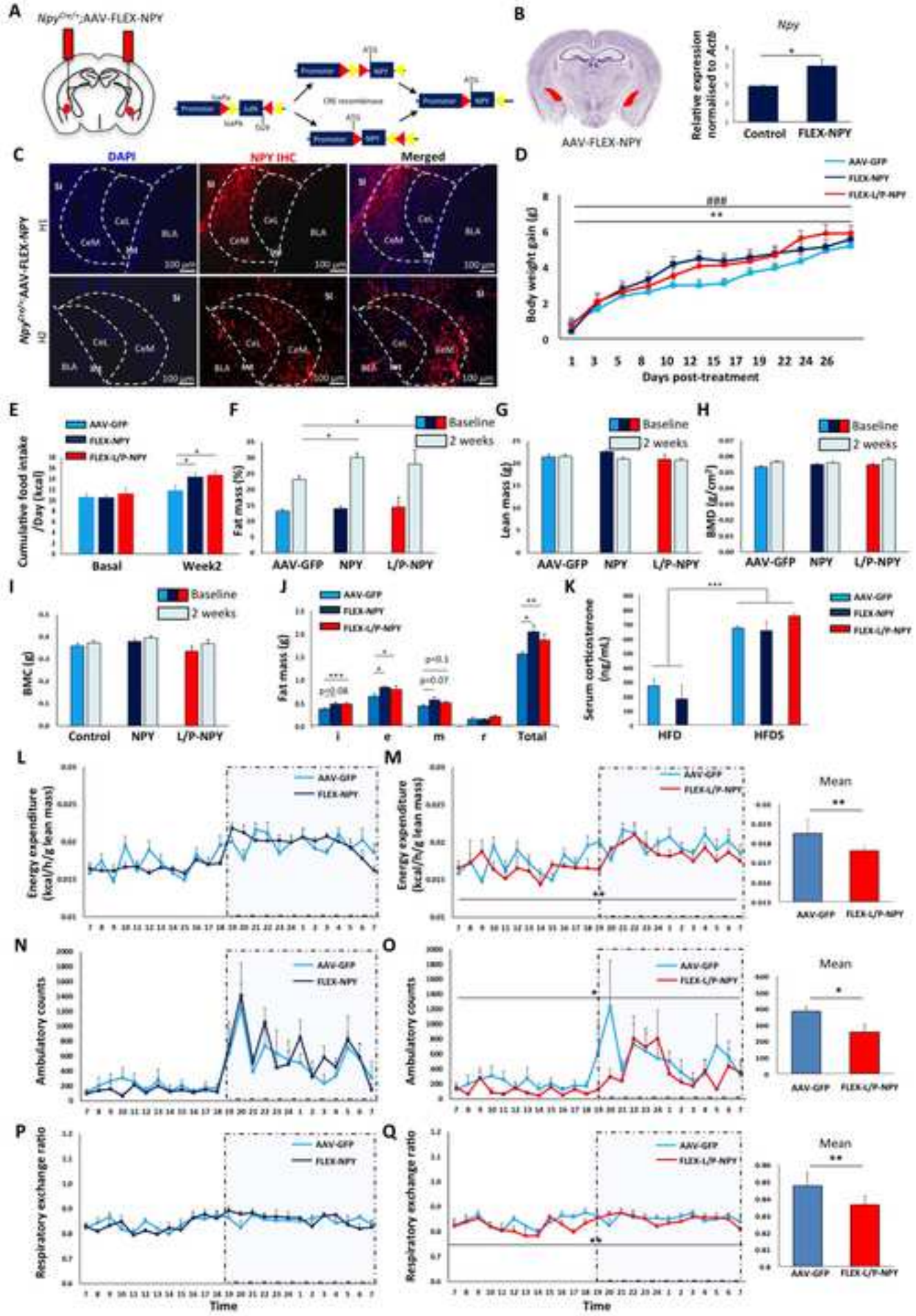

Figure 5

Click here to access/download;Figure;Figure 5.jpg

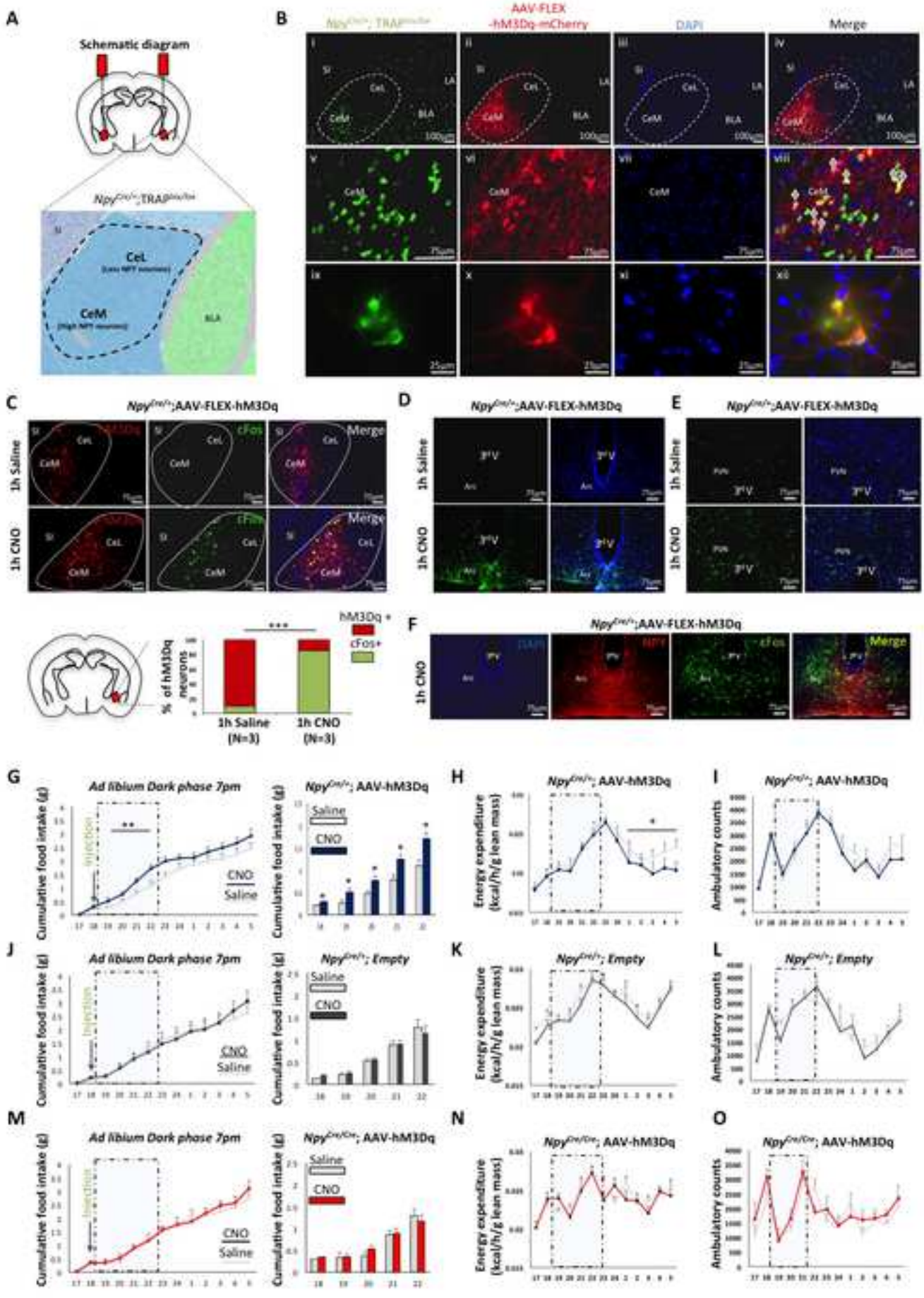

Figure 6

Click here to access/download;Figure;Figure 6.jpg

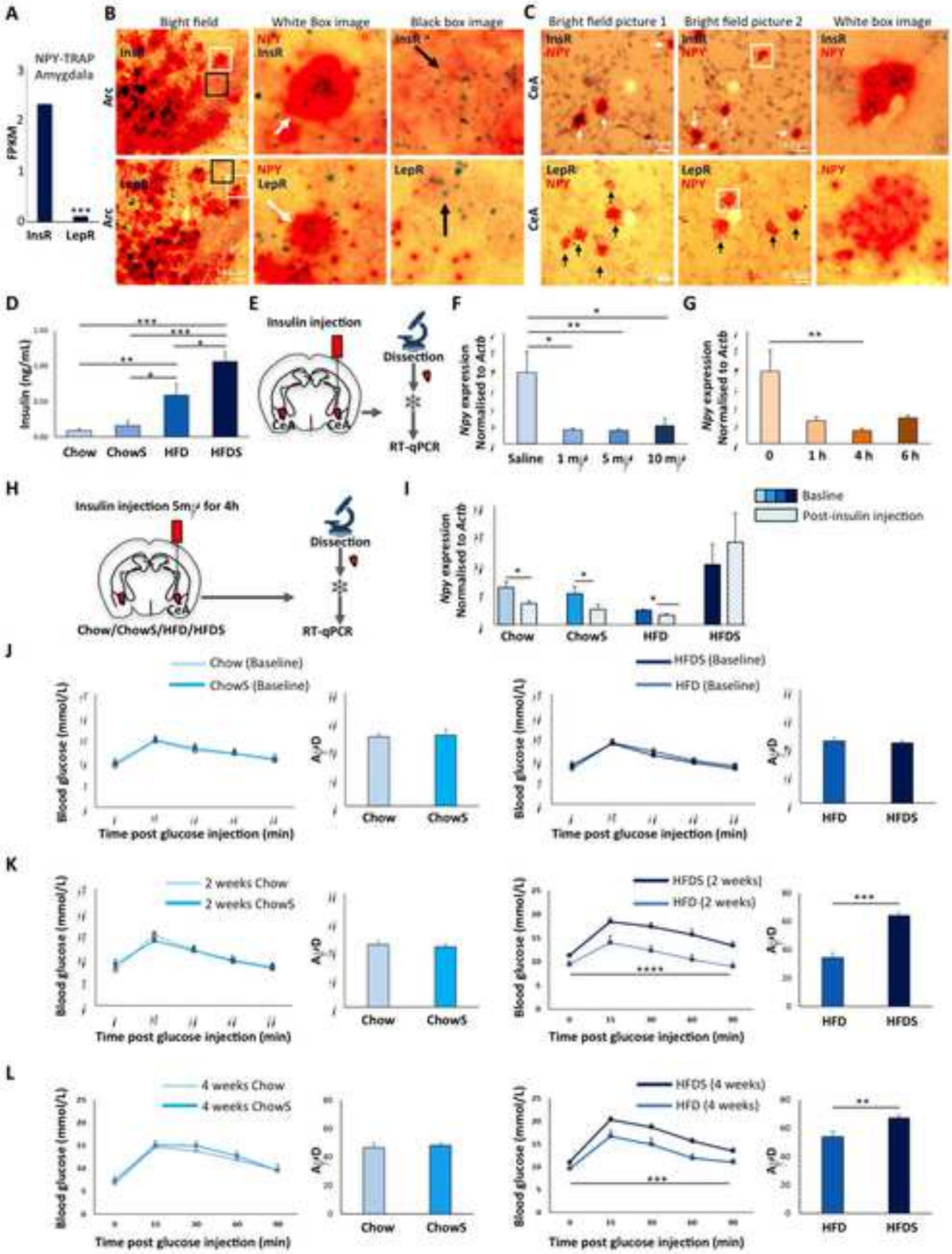

Figure 7

Click here to access/download;Figure;Figure 7.jpg

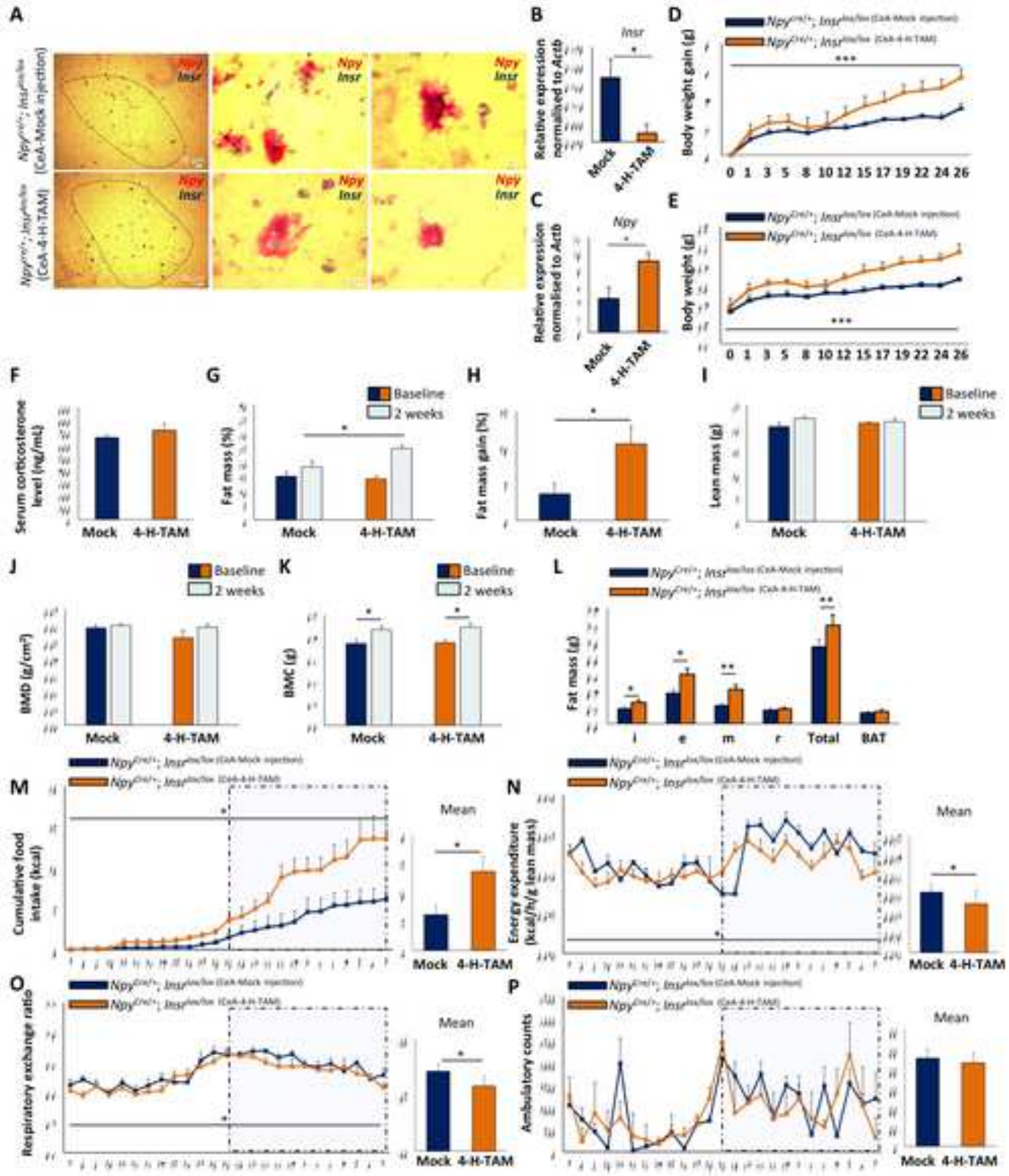

KEY RESOURCES TABLE

KEY RESOURCES TABLE

REAGENT or RESOURCE	SOURCE	IDENTIFIER
Antibodies		
anti-c-Fos polyclonal	Santa Cruz Biotechnologies	Cat# sc-52-G, RRID:AB_2629503
anti-GFP polyclonal	Invitrogen	Cat# A-11122, RRID:AB_221569
tdTomato Polyclonal	SICGEN	Cat# AB8181-200, RRID:AB_2722750
Mouse Monoclonal Anti-NPY	Sigma-Aldrich	Cat# WH0004852M1
Alexa 488 secondaries anti-rabbit	Molecular Probes	Cat# A-11094, RRID:AB_221544
Alexa 488 secondaries anti-goat	Molecular Probes	Cat# A-11073, RRID:AB_142018
Alexa 488 secondaries anti-mouse	Molecular Probes	Cat# A-21202, RRID:AB_141607
RT-PCR associated reagents		
SYBR™ Green I Nucleic Acid Gel Stain	ThermoFisher SCIENTIFIC	Cat# S7563
Platinum™ Taq DNA Polymerase	ThermoFisher SCIENTIFIC	Cat# 10966026
SuperScript™ III First-Strand Synthesis System	ThermoFisher SCIENTIFIC	Cat# 18080051
Chemicals, Peptides, and Recombinant Proteins		
Cycloheximide	Sigma-Aldrich	Cat# C7698
Protease inhibitor	Roche	Cat# 05892791001
RNasin® Ribonuclease Inhibitors	Promega	Cat# N2111
1,2-diheptanoyl-sn-glycero-3-phosphocholine, powder (DHPC)	Sigma-Aldrich	Cat# 850306P
(Z)-4-Hydroxytamoxifen	Sigma-Aldrich	Cat# H7904
Clozapine N-oxide	Sigma-Aldrich	Cat# C0832
Fluoroshield with DAPI	Sigma-Aldrich	Cat# F6057
Commercial assays or kit		
Sensitive Rat Insulin RIA	Merck Millipore	Cat# SRI-13K
Corticosterone DA ^{125}I	MP Biomedicals	Cat# 07120102
Dynabeads™ Protein G for Immunoprecipitation	Invitrogen	Cat# 10004D
RNeasy Micro Kit	Qiagen	Cat# 74004

SuperScript™ III First-Strand Synthesis System	Thermofisher	Cat# 18080051
RNAscope® 2.5 HD Duplex Detection Kit (Chromogenic)	ACD	Cat# 322500
Software and Platform		
GraphPad Prism 6 for Mac OS X	GraphPad Software	Graphpad Prism, RRID:SCR_002798
SPSS for Mac OS X version 16.0.1	SPSS Inc	SPSS, RRID:SCR_002865
LightCycler Software	LightCycler Software	LightCycler Software, RRID:SCR_012155
FLIR thermocamera T640	FLIR	MODEL: T640
Deposited data		
TRAP-seq raw data from Input and IP RNA isolated from the *Npy*$^{Cre/+}$;TRAP$^{lox/lox}$ mice	NCBI GEO	GEO: GSE128413
Experimental models: **Mus** musculus		
B6;129S4-Gt(ROSA)26Sortm9(EGFP/Rpl10a)Amc/J Mus musculus (TRAP mouse)	JAX	Cat# JAX:024750, RRID:IMSR_JAX:024750
NPY-hrGFP	JAX	JAX Cat#006417
C57 Black (C57BL/6J)	JAX	JAX Cat#000664
Npy$^{icre/+}$	Shi et al., 2013	
Npy$^{lox/lox}$	Shi et al., 2013	
Insr$^{lox/lox}$	Bruning et al., 2000	

Supplemental Figures 1

Click here to access/download;Supplemental Text and Figures;Sup figure 1.jpg

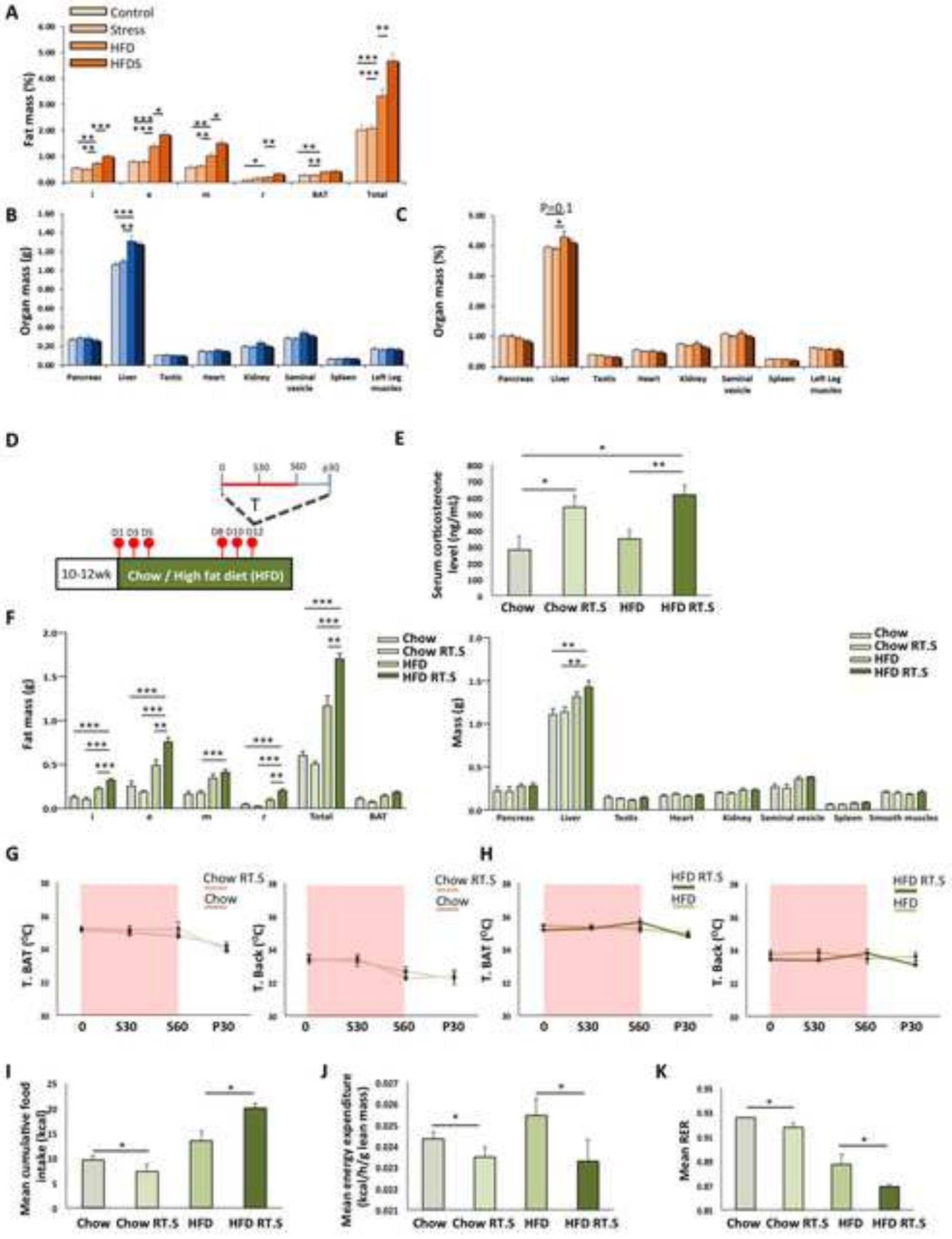

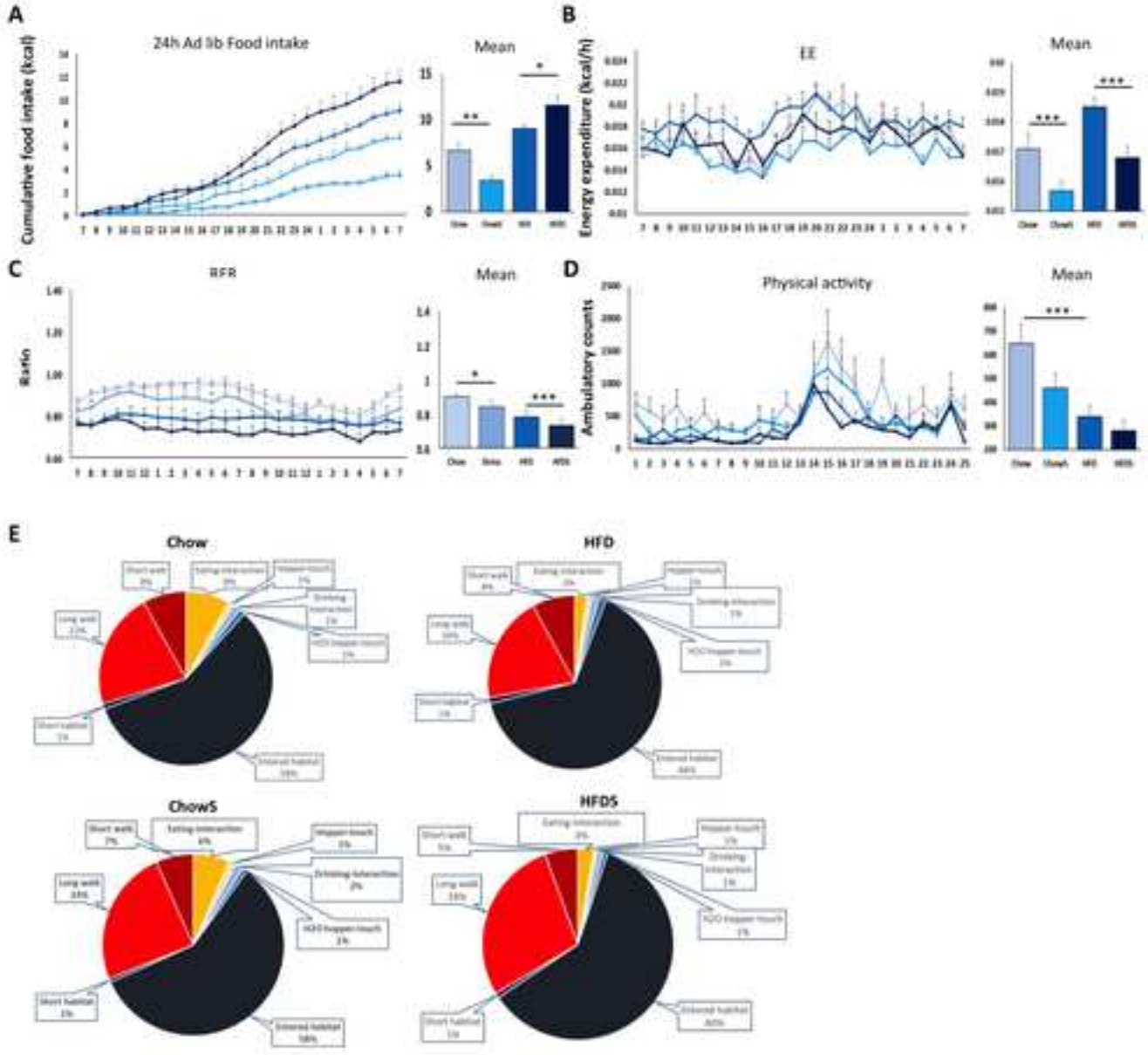

Supplemental Figures 3

Click here to access/download;Supplemental Text and Figures;Sup figure 3.jpg

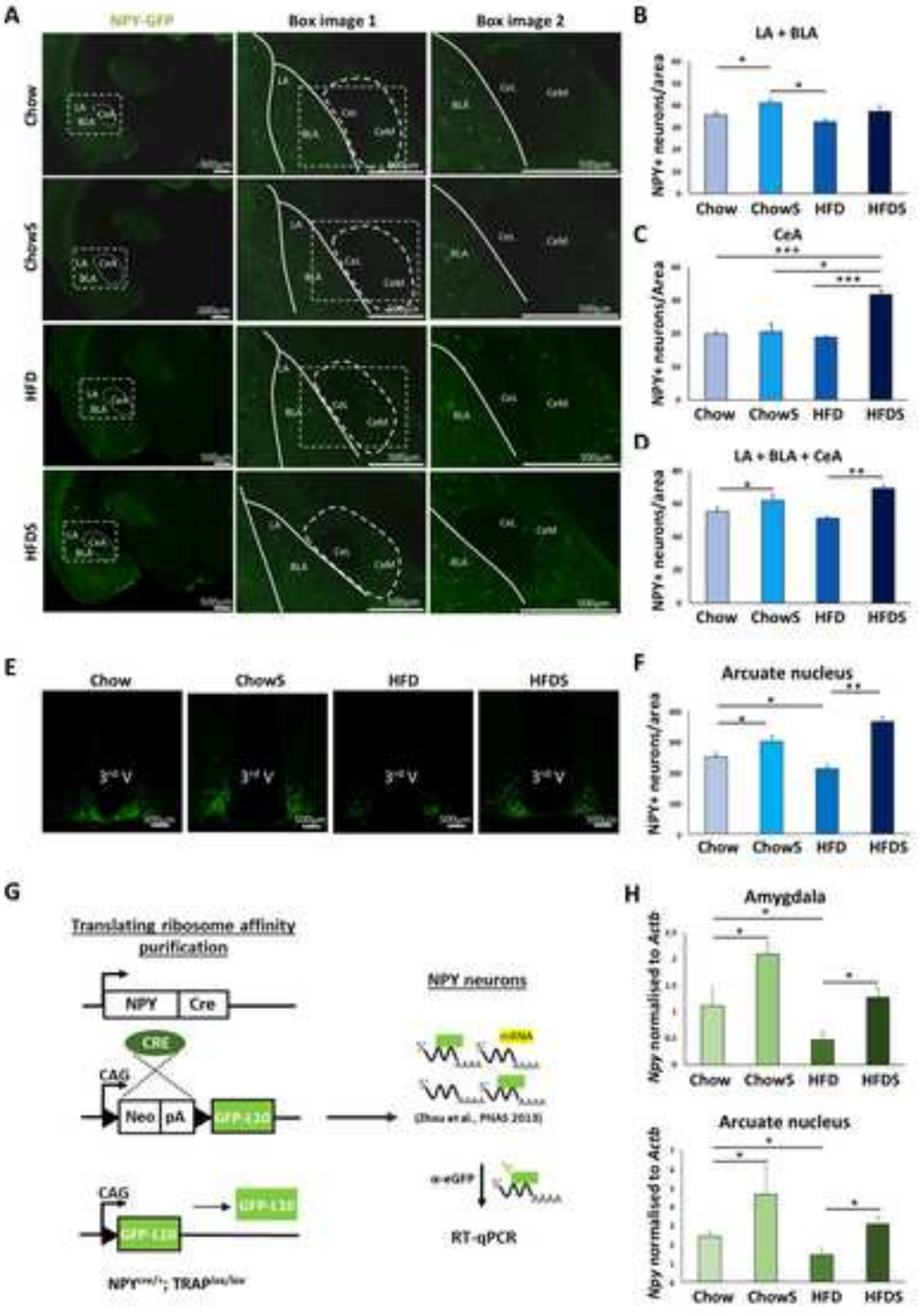

Click here to access/download;Supplemental Text and Figures;Sup figure 4.jpg

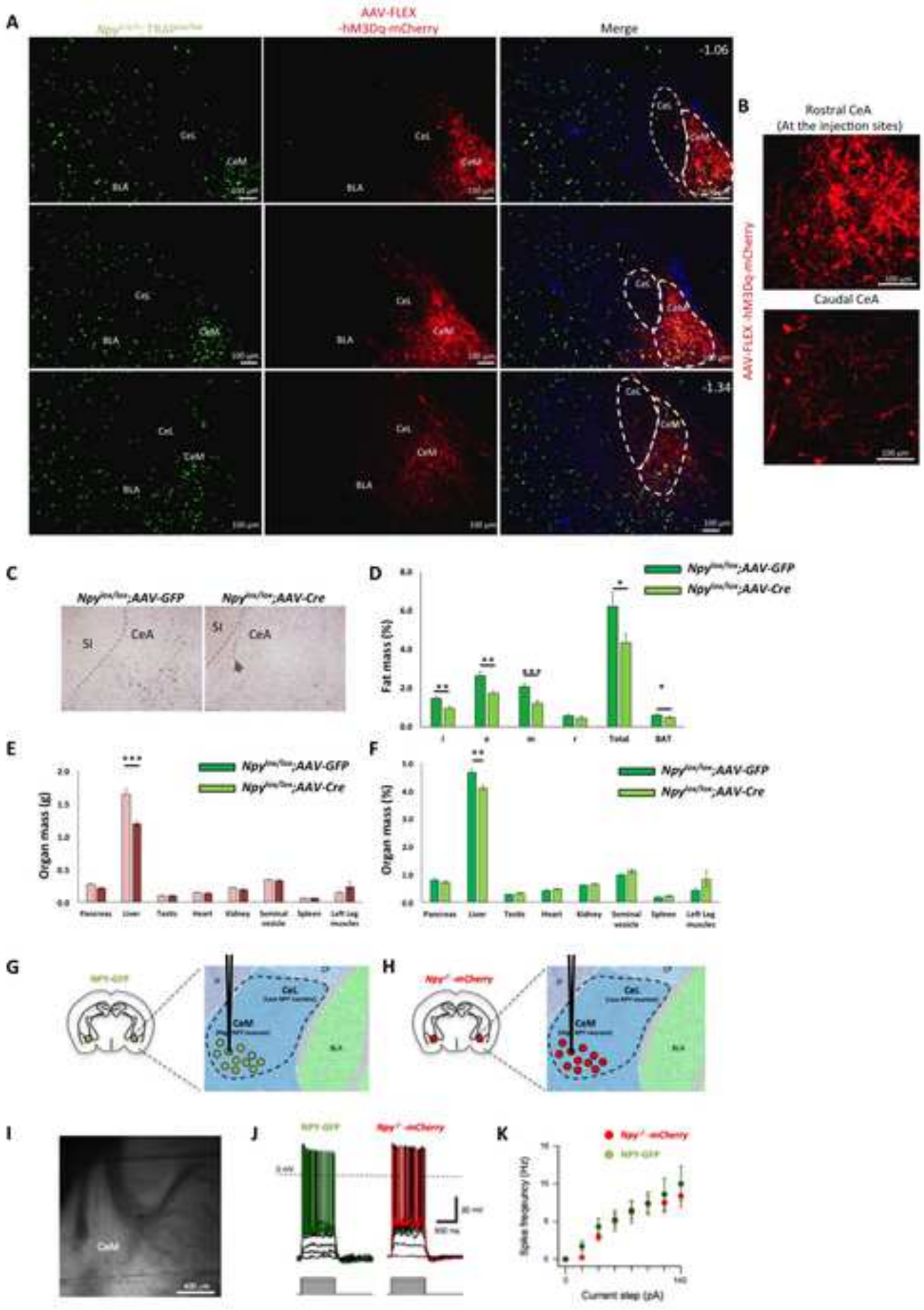

Supplemental Figures 5

Click here to access/download;Supplemental Text and Figures;Sup figure 5.jpg

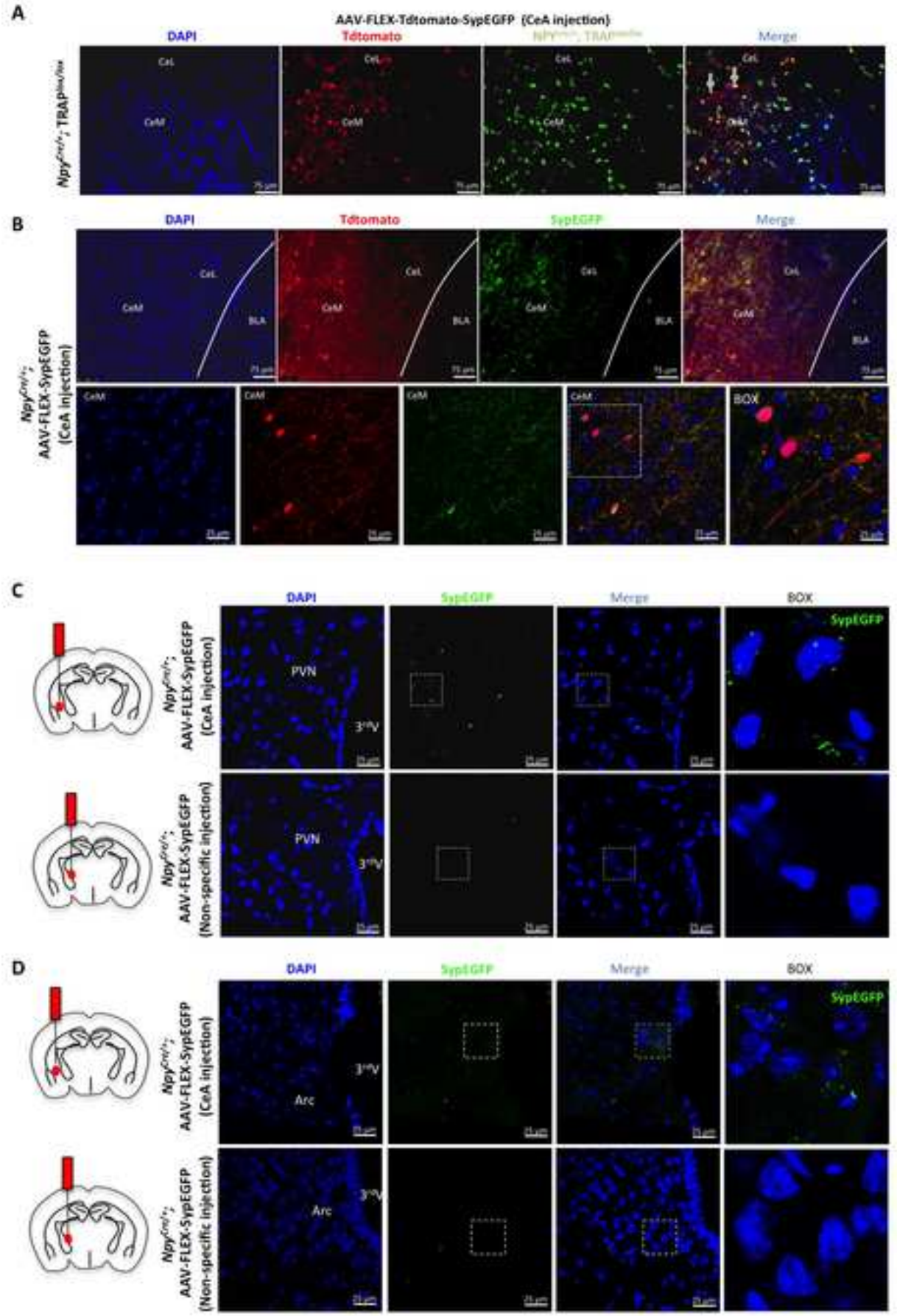

Supplemental Figures 6

Click here to access/download;Supplemental Text and Figures;Sup figure 6.jpg

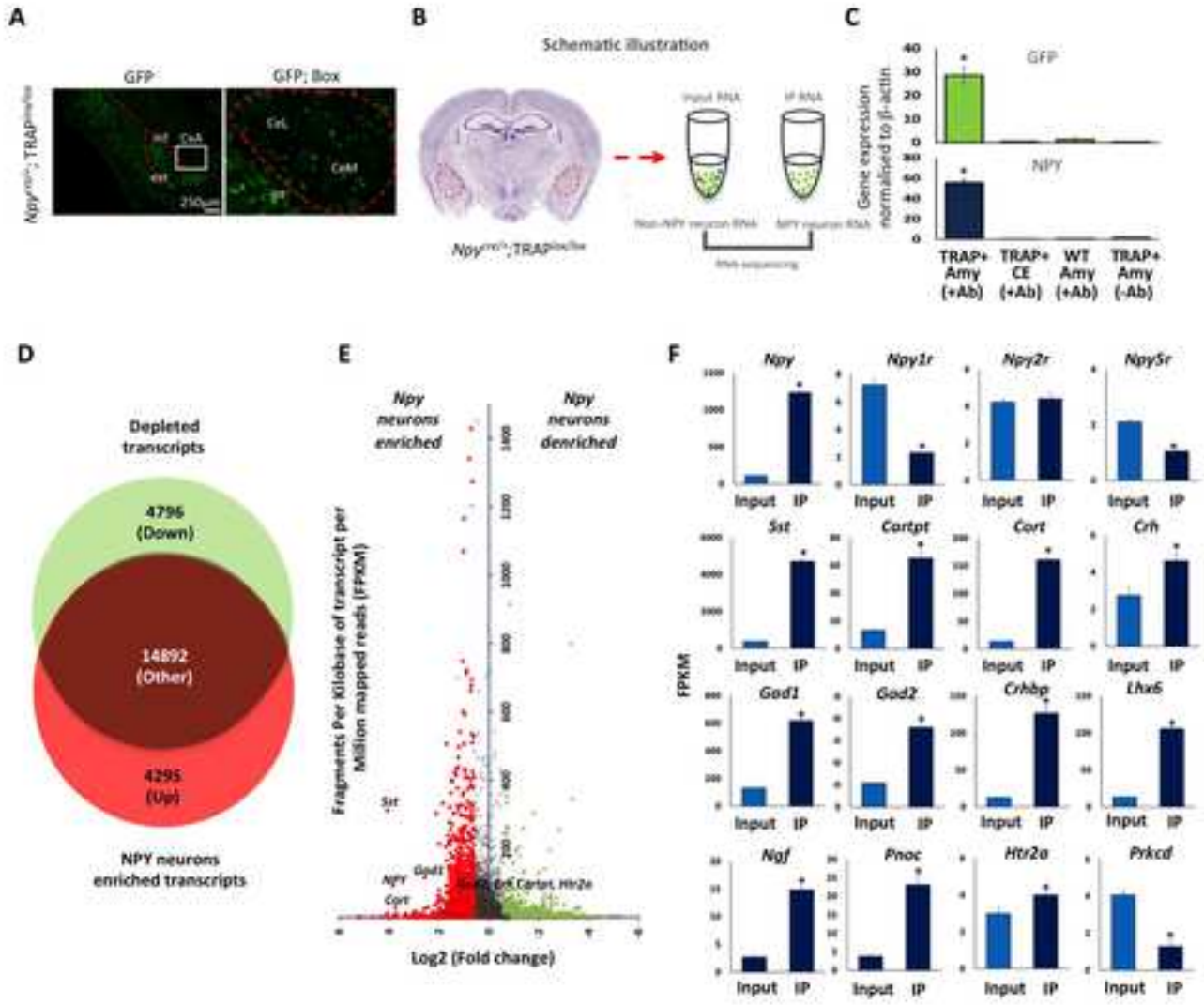

Supplemental Figures 7

Click here to access/download;Supplemental Text and Figures;Sup figure 7.jpg

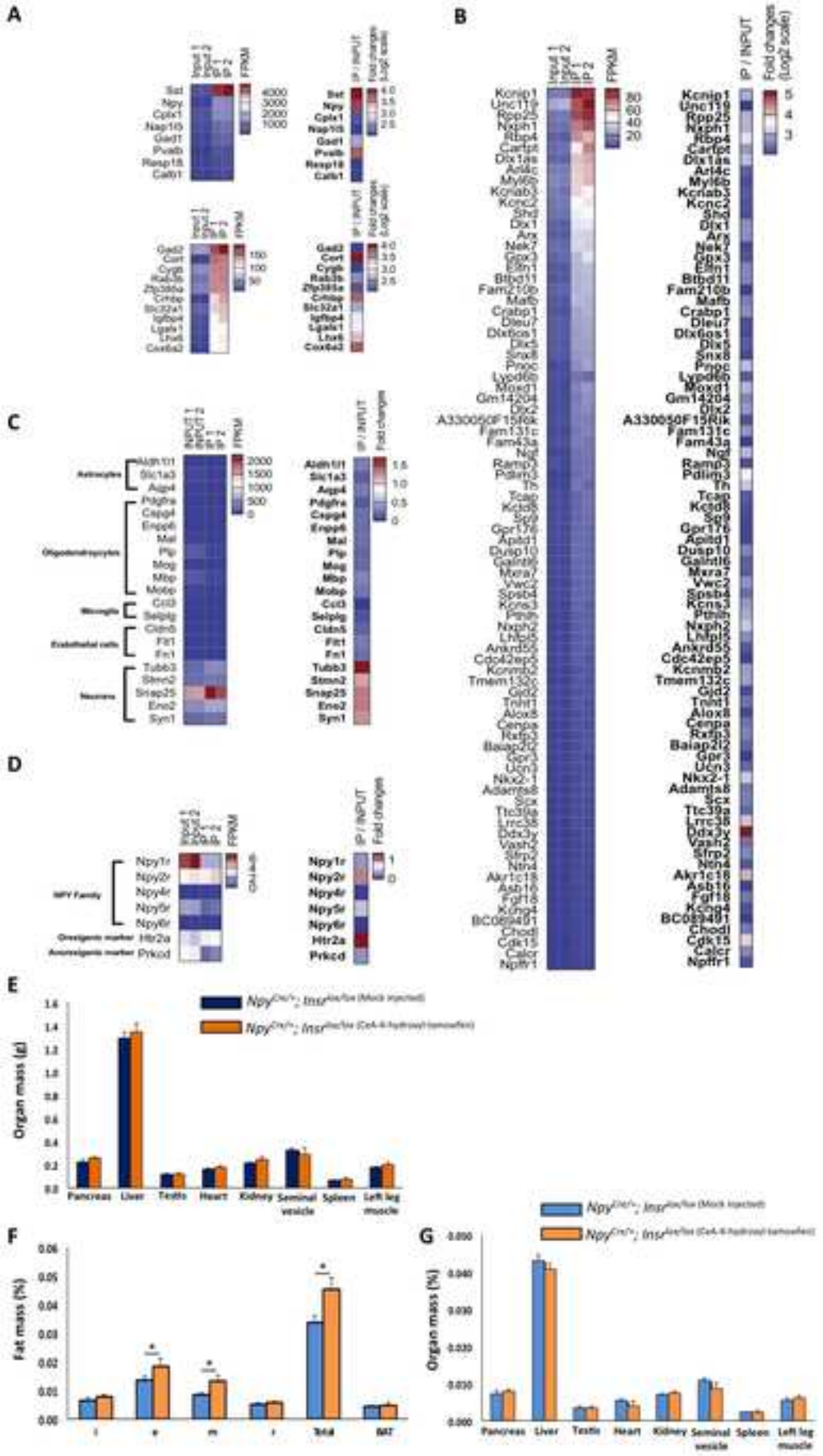

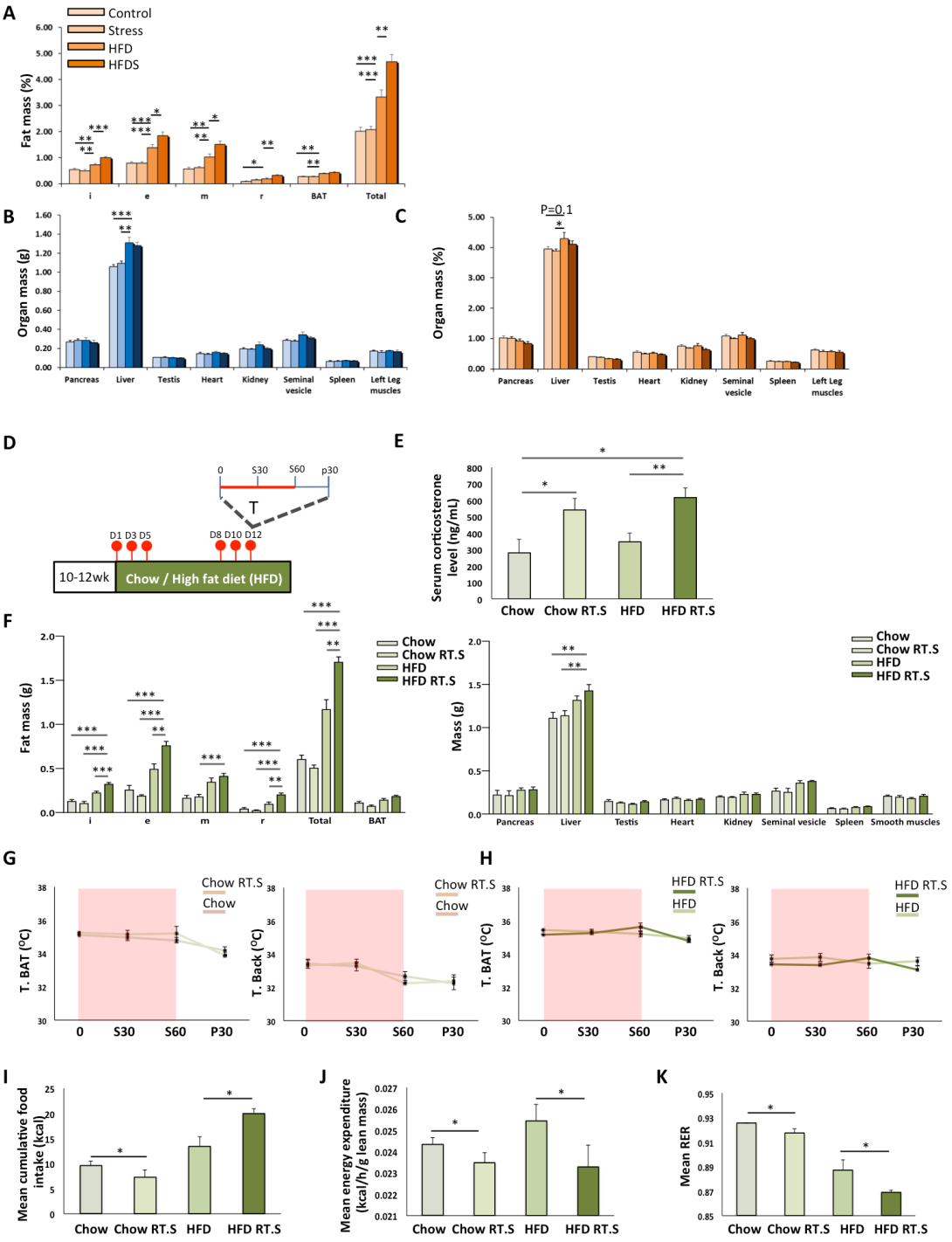

Supplementary figure 1. Related to Figure 1. (A) Weight of white adipose depots of all 4 different mouse models normalised to body weight including inguinal fat (i), epididymal (e), mesenteric (m), and perirenal fat (r), BAT and sum of total fat mass (Total). (B) Absolute and (C) normalized weights of different organs and tissues. Data are means ± SEM, 8-12 mice per group. (D) Schematic Illustration of the two weeks chronic stress phenotyping paradigm and the corresponding metabolic profiling and body composition monitoring done at baseline and two weeks after the treatment. Red dots represent 1h stress treatment. T

indicates body temperature measurement done from time 0 to post-stressed 30 min. S30, stressed for 30 min, S60, stressed for 60 min, +30, 30 min after stressed. (E) Serum corticosterone level in Chow, Chow RT.S (Room temperature water stress), HFD and HFD RT.S group. Data are means ± SEM, 5-8 mice per group. (F) Weight of dissected white adipose depots, inguinal fat (i), epididymal (e), mesenteric (m), perirenal fat (r) and summed total fat mass and BAT and absolute weights of different organs and tissues from mice of the different treatment groups using water at room temperature. Data are means ± SEM, 5-8 mice per group. (G, H) Temperature of the BAT (T-BAT) and lumber back (T-Back) region in mice of the Chow, Chow RT.S, HFD and HFD RT.S group during the 1 h stress paradigm and 30 min post-stress treatment. 0, 0 h; S30, stressed for 30 min; S60, stressed for 60 min; P30, post-stress at 30 min. Data are means ± SEM, 5-8 mice per group. *P<0.05; **P<0.01; ***P<0.001. (I) 24h cumulative caloric intake for Chow, Chow N.S., HFD and HFD N.S. mice, (J) Energy expenditure, (K) Respiratory exchange ratio accessed 2 weeks after the commencement of the phenotyping paradigm. Data are means ± SEM , 4 mice per group.

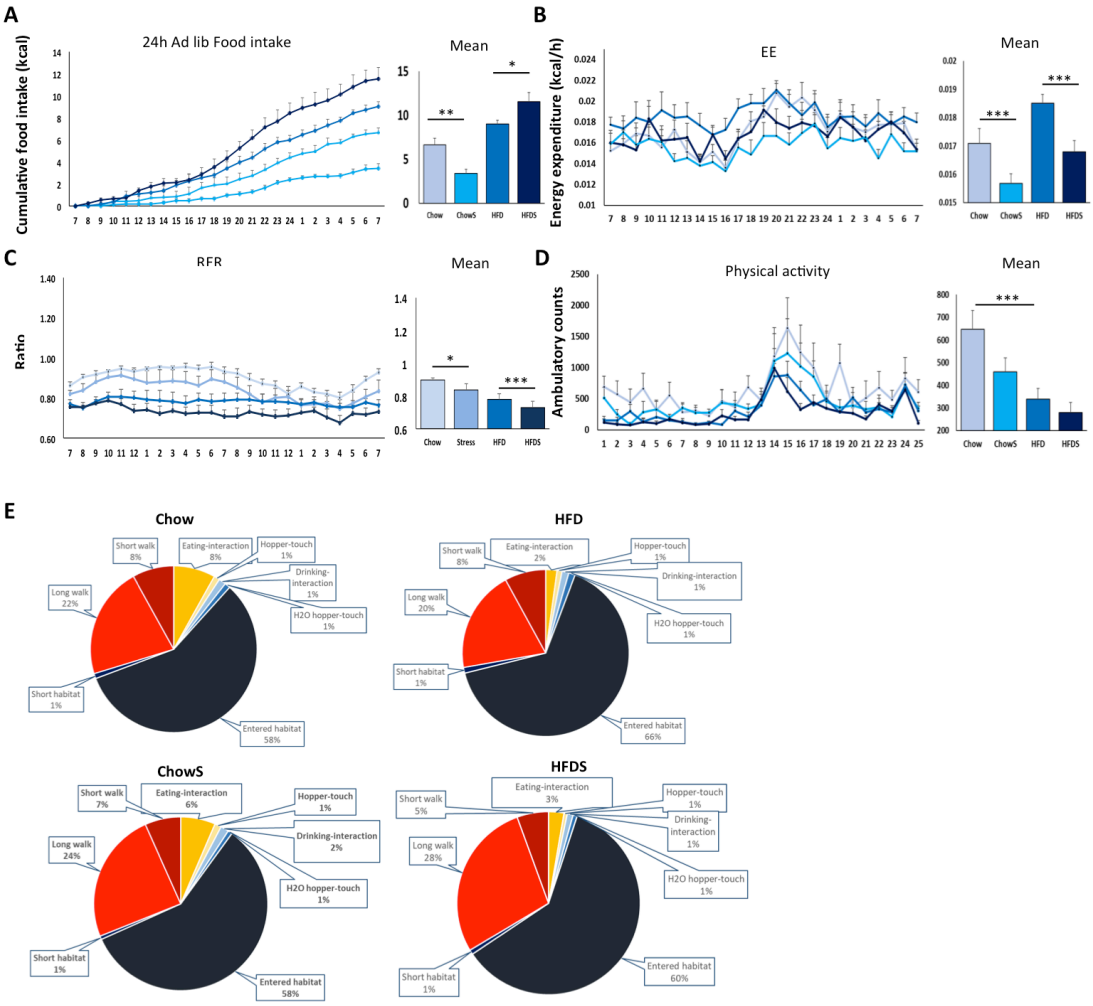

Supplementary figure 2. Related to figure 2. (A) Cumulative food intake of the whole 24h monitoring period. Data are represented as means ± SEM, 4 mice per group. (B-D) Energy expenditure, respiratory exchange ratio and ambulatory counts. Bar graphs show the data means of the whole 24h period. Data are represented as means ± SEM, 8-12 mice per group. (E) Activity catagorisation of individual Chow, ChowS, HFD, HFDS mice during the full physiology monitoring section. Pie chart for the quantification of different activities determined by the Promethion system expressed as a percentage of the overall activity.

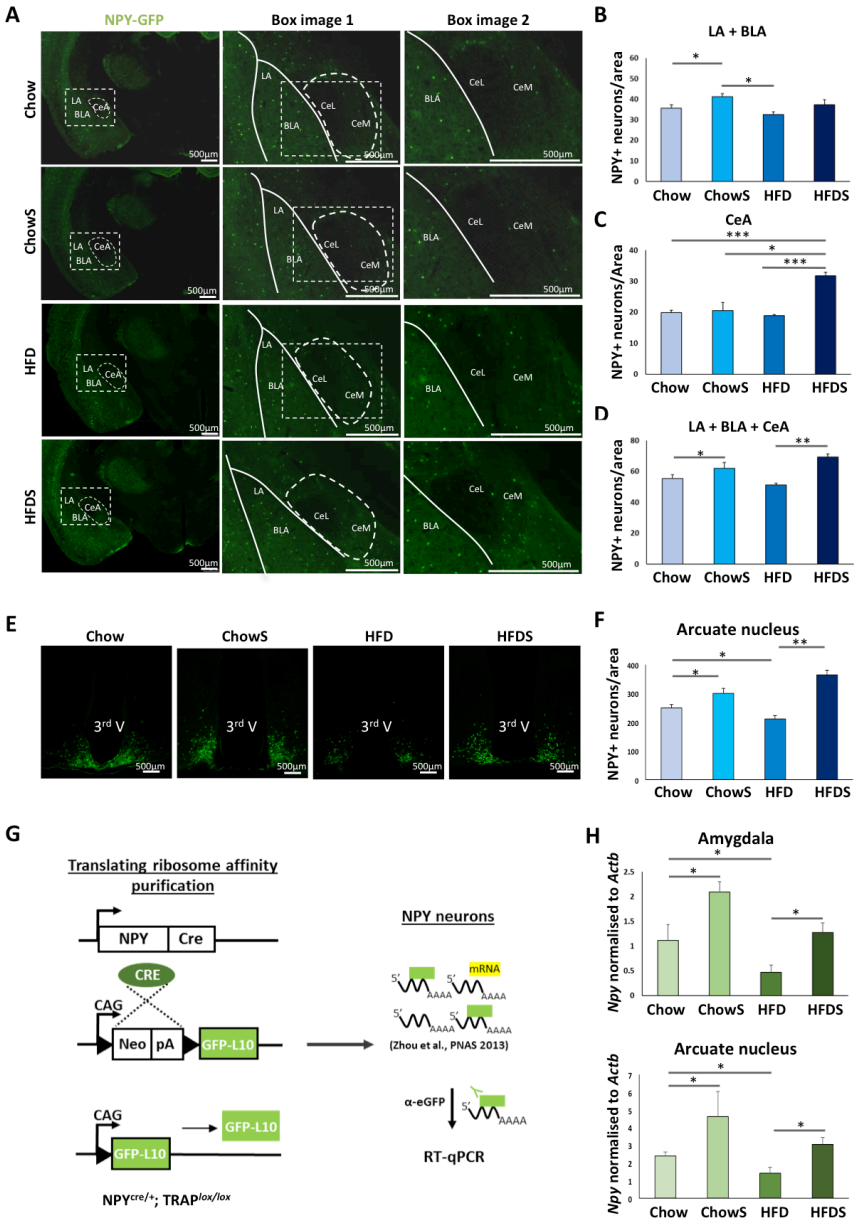

Supplementary figure 3. Related to Figure 3. (A) Distribution of NPY in neurons in different sub-nuclei of the amygdala visualised by GFP expression controlled by the NPY promotor. LA, lateral amygdala; BLA, basolateral amygdala; CeA, central amygdala; CeI, centrolateral amygdala; CeM, centromedial amygdala. Magnified in boxed images. Scale bar, 500 µm. (B, C) Number of GFP positive NPY neurons (GFP+) in the LA, BLA and CeA under Chow, ChowS, HFD and HFDS conditions. (D) Number of GFP positive NPY neurons (GFP+) counted in the whole amygdala (LA + BLA + CeA). (E) Expression of NPY neurons in the arcuate nucleus. 3rd V = 3rd ventricle. (F) Number of GFP positive NPY neurons (GFP+) in the arcuate nucleus under Chow, ChowS, HFD and HFDS conditions. Data are means ± SEM, 3-5 mice per group. (G) Illustration of the "translating ribosome affinity purification" (TRAP) technology combined with RT-qPCR analysis. (H) Enrichment of *Npy* transcripts normalised to *Actb* in

the immunoprecipitated RNA of the amygdala and arcuate nucleus of *Npy*$^{Cre/+}$;TRAP$^{lox/lox}$ mice treated with the Chow, ChowS, HFD or HFDS paradigm. Data are means ± SEM, 3-5 pairs of amygdala per group. * P<0.05; **P<0.01; ***P<0.001.

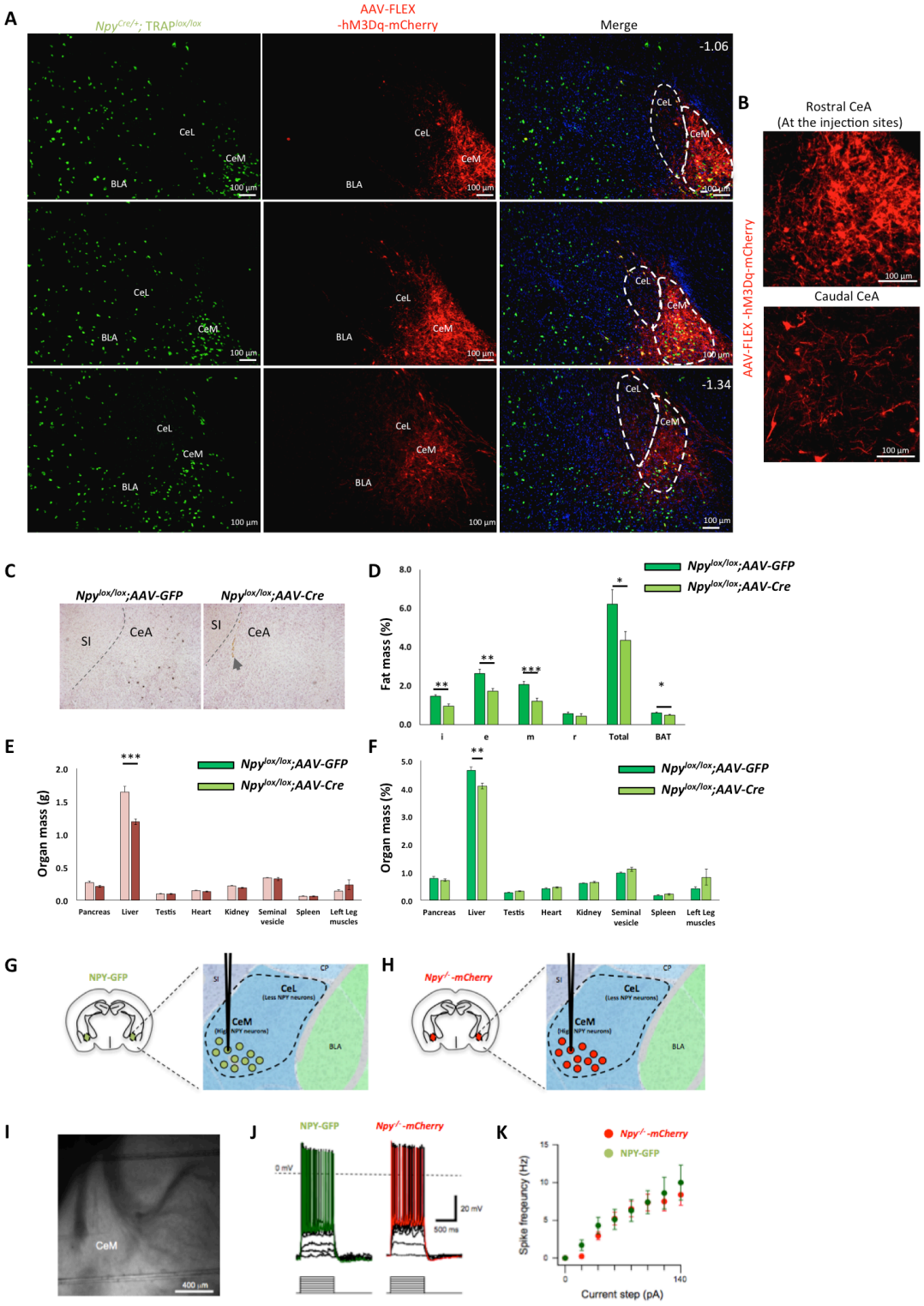

Supplementary figure 4. Related to Figure 3 and 5 (A) Validation of the expression pattern of Cre-dependent AAV-hM3Dq-mCherry in *Npy*$^{Cre/+}$ mice for CNO-induced neuronal activation. Fluorescence micrographs of coronal brain sections covering the CeA region relative to Bregma at -1.06 mm, -1.22 mm and -1.34 mm (Franklin and

Paxinos, 1997). BLA, basolateral amygdala; CeM, medial nuclei of the central amygdala; CeL, lateral nuclei of central amygdala. (B) Expression of AAV-hM3Dq-mCherry at the injection site and at the caudal CeA where only neuron fibres are found. (C) Photomicrograph of *in situ* hybridization of photoemulsion dipped sections showing *Npy* mRNA expression in the CeA of $Npy^{lox/lox}$;AAV-GFP and $Npy^{lox/lox}$;AAV-Cre mice. SI, substantia innominate, CeA, central amygdala. Grey arrow points to needle track. (D) BAT and WAT tissue weights including inguinal fat (i), epididymal (e), mesenteric (m), and perirenal fat (r) from $Npy^{lox/lox}$;AAV-GFP and $Npy^{lox/lox}$;AAV-Cre mice normalised to body weight, and summed WAT depots. (E, F) Dissected organ and tissue weights normalised to body weight. Data are means ± SEM, 10-11 mice per group. * P<0.05; **P<0.01; ***P<0.001. (G, H) Schematic Illustration of NPY neurons recording in the CeM. (I) Image shows CeA brain slice with recording pipette positioned in the medial division of CeA. (J) Representative AP discharge responses recorded from CeA neurons in tissue from NPY-GFP (left) and $Npy^{Cre/Cre}$ (right) animals during current step injections (lower - 20pA increments, 900ms duration). (K) Plots shows group data summarizing F/I relationship between AP discharge and current injection in NPY-GFP (n=15) and $Npy^{Cre/Cre}$ (n=14) recordings. Responses are unchanged in the absence of NYP ($Npy^{Cre/Cre}$).

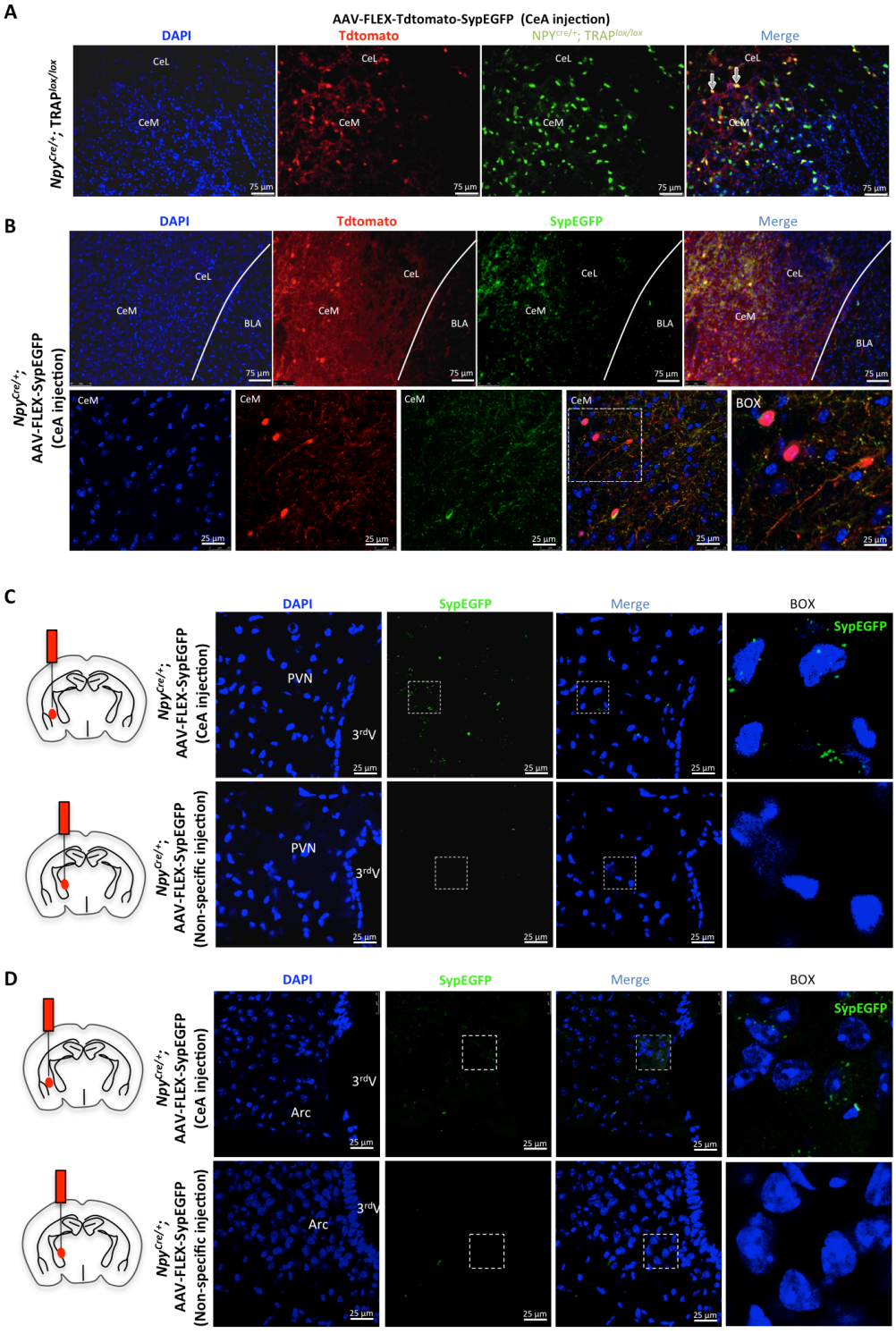

Supplementary figure 5. Related to Figure 5. (A) AAV-FLEX-Tdtomato-SypEGFP visualization in the medial nuclei of the central amygdala (CeM) of *Npy*$^{Cre/+}$;TRAP$^{lox/lox}$ mice. Yellow staining represents expression of AAV-FLEX-Tdtomato-SypEFP in NPY cells. Arrows point to example of yellow stained cells. (B top panels) Visualisation of AAV-FLEX-Tdtomato-SypEGFP expressing cells with Tdtomato (Red) and EGFP-fused

synaptophysin (SypEGFP) expressing neuron cell bodies and fibres. (B lower panels) Higher magnification of fluorescent micrograph showing Tdtomato-labelled neuron cell bodies and SynEGFP expressing neuron fibres in the CeM of *Npy*$^{Cre/+}$;AAV-FLEX-Tdtomato-SypEGFP mice. (C, D) Fluorescent micrographs by confocal microscopy showing SynEGFP projecting fibres in both PVN and Arc of the *Npy*$^{Cre/+}$ mice expressing AAV-FLEX-Tdtomato-SypEGFP construct in the CeA but not in the *Npy*$^{Cre/+}$ mice expressing AAV-FLEX-Tdtomato-SypEGFP construct in the lateral thalamus. BLA, basolateral amygdala; CeA, central amygdala; CeI, centrolateral amygdala; Cem, centromedial amygdala; Arc, arcuate nucleus.

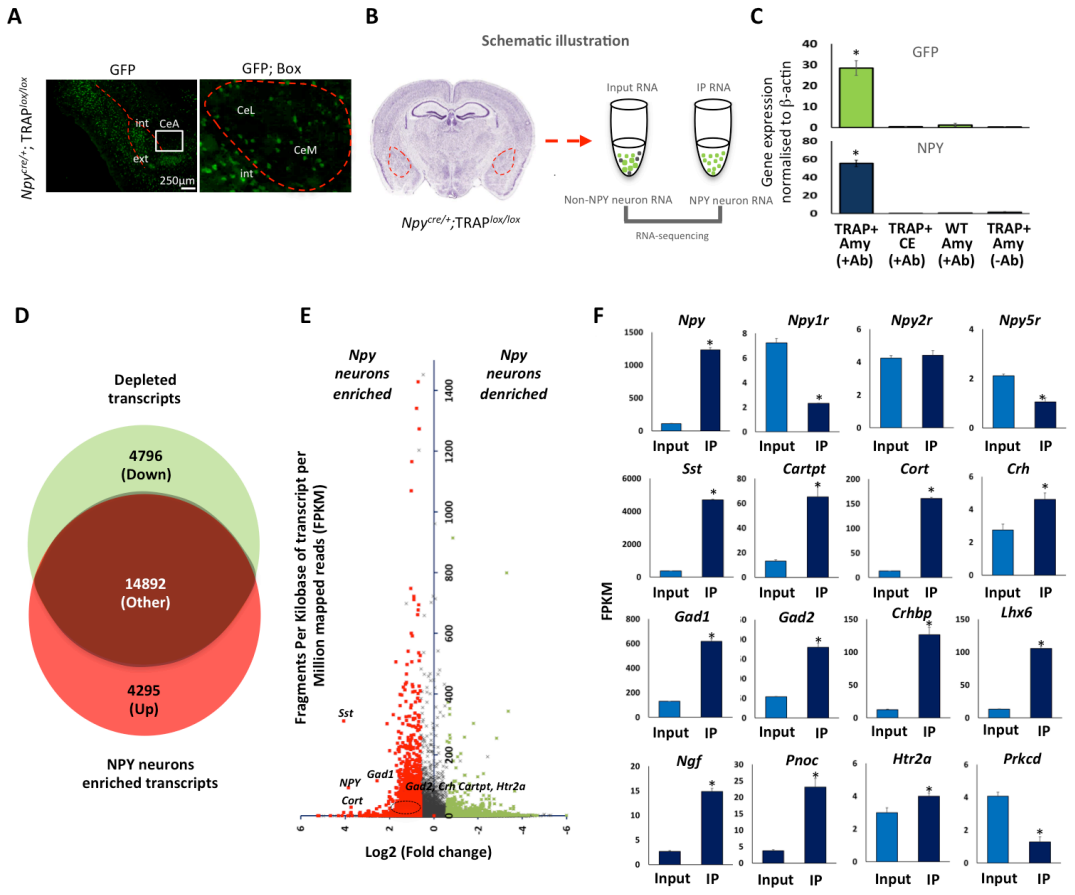

Supplementary figure 6. Related to Figure 3, 4 and 5. (A) Visualisation of fluorescent NPY neurons in the amygdala of *Npy*$^{Cre/+}$;TRAP$^{lox/lox}$ mice. (B) Schematic of TRAP-sequencing approach using *Npy*$^{Cre/+}$;TRAP$^{lox/lox}$ mice. (C) Enrichment of GFP and *Npy* transcripts in the immunoprecipitated RNA of the amygdala of *Npy*$^{Cre/+}$;TRAP$^{lox/lox}$ mice (TRAP+ Amy) and the cerebellum of *Npy*$^{Cre/+}$;TRAP$^{lox/lox}$ mice (TRAP+ CE) as well as the amygdala of wild type *Npy*$^{+/+}$;TRAP$^{lox/lox}$ mice (WT Amy). +Ab, immunoprecipitated with an anti-GFP antibody. -Ab, immunoprecipitated without an anti-GFP antibody. Data are means ± SEM, 3-5 pairs of amygdalae per group. * P<0.05; **P<0.01; ***P<0.001. (D) Venn diagram for depleted genes (green part), un-changed genes (Dark brown outlined) and enriched genes (red part) between immunoprecipitated (IP) and input (unprocessed) RNA samples. Reported significant differentially expressed genes between two groups required q-value <0.05, fold change >1.5 fold. (E) Volcano plot represents the TRAP-seq IP data relative to the input data. FPKM on y-axis represents endogenous expression value in input sample of all genes. x-axis represents the changes in the FPKM value of all genes after immunoprecipitation. Red dots are genes with a statistically significant enrichment, green dots are genes with a statistically significant depletion, grey dots are unchanged genes. FPKM, Fragment Per Kilobase of

transcript per Million mapped reads. (F) Bar graph representing a selected group of statistically significant differentially expressed genes. * $P<0.05$.

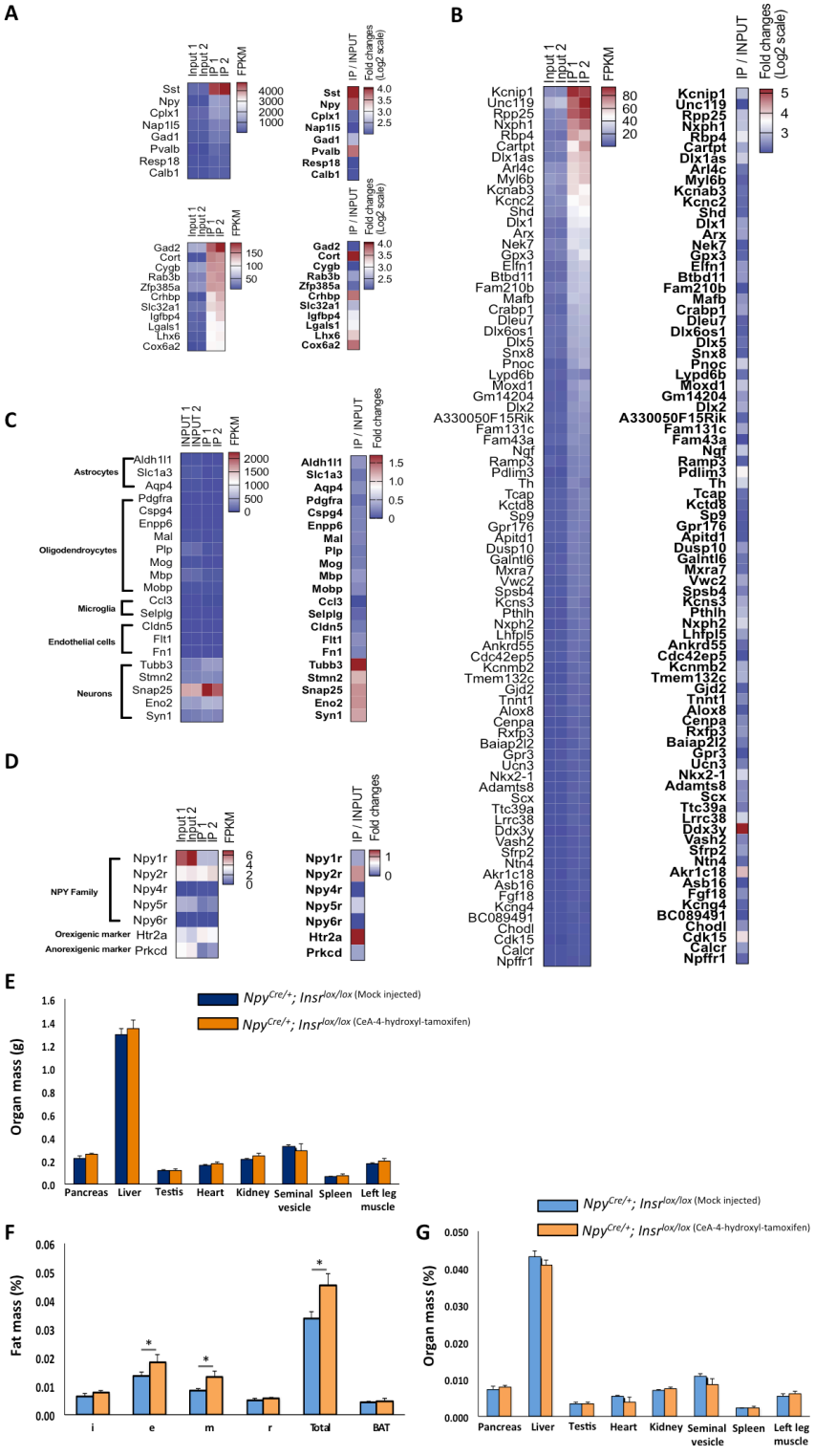

Supplementary figure 7. Extended data from Supplementary figure 6 and related to Figure 7. (A, B) Heatmap represents the 100 most significantly enriched genes in immunoprecipitated (IP) samples of the CeA of *Npy*$^{Cre/+}$;TRAP$^{lox/lox}$ mice. (C) Heatmap shows the expression of marker genes for astrocytes, oligodendrocytes, microglia, endothelial cells and neurons. (D) Heatmap shows the expression of NPY receptor genes and marker gene

that marks the CeA-orexigenic neurons and anorexigenic neurons. Left panel shows raw FPKM and left panel shows fold change compare to Input RNA (Log2 scale). Also See Table S1. (E) Dissected organ and tissue weights of $Npy^{Cre/+};Insr^{lox/lox(CeA\text{-}Mock\ injection)}$.and $Npy^{Cre/+};Insr^{lox/lox(CeA\text{-}4\text{-}H\text{-}TAM)}$. Data are means ± SEM, 4-7 mice per group. (F) BAT and WAT tissue weights including inguinal fat (i), epididymal (e), mesenteric (m), and perirenal fat (r) from $Npy^{Cre/+};Insr^{lox/lox(CeA\text{-}Mock\ injection)}$.and $Npy^{Cre/+};Insr^{lox/lox(CeA\text{-}4\text{-}H\text{-}TAM)}$ mice normalised to body weight, and summed WAT depots. (G) Dissected organ and tissue weights normalised to body weight. Data are means ± SEM, 4-7 mice per group. * P<0.05.

Supplemental table 1